ECOLOGY AND EVOLUTION OF VECTOR-BORNE VIRUSES: EMPIRICAL AND MATHEMATICAL APPROACHES TO UNDERSTANDING THE PERSISTENCE OF CLINICALLY IMPORTANT ARBOVIRUSES

By

GABRIELA MAXINE BLOHM

A DISSERTATION PRESENTED TO THE GRADUATE SCHOOL
OF THE UNIVERSITY OF FLORIDA IN PARTIAL FULFILLMENT
OF THE REQUIREMENTS FOR THE DEGREE OF
DOCTOR OF PHILOSOPHY

UNIVERSITY OF FLORIDA

2017

To my grandparents

ACKNOWLEDGMENTS

I thank my parents, Mary Lou Adams de Blohm and Jorge Tomas Blohm, for teaching me to constantly push myself. I thank my siblings, Melissa, Melanie and John Robert, for supporting, inspiring and challenging me in ways that have helped me grow. My grandfather Tomas Blohm and my grandmother Cecilia Montemayor de Blohm sparked my interest in the sciences, thus I would not have pursued this professional direction without their influence.

I am thankful every day for the support, encouragement, loyalty and friendship of my partner Juan Carlos Oteyza and our dog Zamba.

I thank Jose Miguel Ponciano for his dedication to thinking rigorously and to his patience in teaching me how to connect models and biology. I will be eternally thankful for his encouragement and for his influence as a mentor. I also thank Marta Wayne for giving me the opportunity to pursue research, for her friendship, and for her influence on my personal and professional growth. I thank Jim Maruniak for his friendship, kindness and for opening the doors to his lab so that I could learn how to work with cells. I thank Barry Alto for running a research lab that is focused on problem-solving, cooperation and scientific rigor. I learned so much while watching him manage the complexities – both scientific and logistical – of running a BSL-3 laboratory. I also thank him for providing me with the opportunity to gain experience working with cells and WNV in the BSL-3. I thank Mike Miyamoto for his insights and encouragement throughout the development of my dissertation. I thank Juliet Pulliam for her influence on my intellectual development, and for showing me that it's possible to combine basic and applied research for solving public health problems.

I thank the students that helped me collect flies in Georgia and run experiments in the Wayne lab. I am thankful to Kylie Zirbel and Eva Buckner for their help and guidance at FMEL. Maia Martcheva and Hayriye Gulbudak from the Department of Mathematics at the University

of Florida contributed to the development of the mathematical models on West Nile Virus replication. The work in Venezuela would not have been possible without Dr. Alberto Paniz-Mondolfi, whose commitment to alleviating our humanitarian crisis is unshakeable. I thank John Lednicky, Glenn Morris, Julia Loeb, Sarah White and Tania Bonny for letting me work in their lab, for their insights on experimental design and virus isoloation, and for helping me build a bridge towards the work I hope to do in the future in Venezuela.

Finally I thank Lucy, my loyal companion through most of this process. I thank uncle Kenny for being an endless source of encouragement and support in my life. I also thank the Venezuelans who risked their lives to bring peace and order back to our beautiful country.

TABLE OF CONTENTS

page

LIST OF TABLES

LIST OF FIGURES

Abstract of Dissertation Presented to the Graduate School
of the University of Florida in Partial Fulfillment of the
Requirements for the Degree of Doctor of Philosophy

ECOLOGY AND EVOLUTION OF VECTOR-BORNE VIRUSES: EMPIRICAL AND MATHEMATICAL APPROACHES TO UNDERSTANDING THE PERSISTENCE OF CLINICALLY IMPORTANT ARBOVIRUSES

By

Gabriela Maxine Blohm

August 2017

Chair: Jose Miguel Ponciano
Major: Zoology

Understanding the factors that allow the establishment and transmission of vector-borne viruses is important for developing effective intervention strategies. In this dissertation, I combine field surveys, laboratory experiments and mathematical models to determine 1) how transmission mode (i.e. vertical transmission vs. horizontal transmission) can affect the persistence of a parasite; 2) how non-living environmental factors (specifically nutrient enrichment) can affect the replication of arboviruses, and 3) how host-level biological factors such as prior exposure to infection can affect disease severity and transmission rate. Results suggest that vertical transmission is an evolutionarily stable strategy, even when it brings a reduction in host fecundity. Laboratory experiments on the effects of phosphorus on replication of West Nile Virus reveal that phosphorus is a growth-limiting factor for cells; however it does not limit the replication of the virus. Mathematical models and simulations of West Nile Virus replication allow us to identify areas in the replication cycle that can be effective targets for antiviral therapies. Findings from field-based surveillance studies of arbovirus prevalence in Venezuela reveal that *Zika virus* can be transmitted perinatally, suggesting that disease

surveillance and vector control should be coupled with basic clinical virology research on arbovirus prevalence.

CHAPTER 1
INTRODUCTION

The geographic range of arthropod-borne viruses (arboviruses) such as *Yellow Fever virus* (YFV), *Dengue virus* (DENV), *West Nile virus* (WNV), *Chikungunya virus* (CHIKV) and *Zika virus* (ZIKV) has increased rapidly (Taylor 2008, Weaver 2010, Patterson 2016). Human migration, global changes in temperature and precipitation cycles, urbanization and agricultural development have facilitated the geographic expansion of DENV, CHIKV and ZIKV (reviewed in Mayer 2017). Successful establishment of these viruses depends on several factors such as virulence, mode of transmission, susceptibility of the host and of the vector, and the epidemiological role of the host (e.g. as a reservoir, amplifier, or sink), among others (Weaver 2010, Mayer 2017). Because these factors operate at vastly different scales of biological organization, it is useful to combine a diversity of approaches when attempting to explain the recent geographic expansion of arboviruses (Lord 2014). Model systems, experimental studies, field surveys, mathematical models and statistical tools are among the approaches that can be combined to improve our ability to predict and control arboviruses. In this dissertation, I use a multidisciplinary approach to explore how virulence, transmission mode and environmental context can affect the emergence of arboviruses.

Virulence – the reduction in host fitness by a parasite (Read 1994), can affect the persistence of a parasite. If the virulence of a parasite is high, it is expected that the opportunities for transmission will decrease due to a reduction in the fitness of the host (Ebert 1999). This tradeoff between virulence and transmission provides an explanation for the persistence of many vector-borne viruses, where the vectors are thought to experience a relatively small reduction in fitness when infected (Lambrechts 2009). Within the vector population, arboviruses can be transmitted horizontally (e.g. orally when the vector is obtaining an infectious bloodmeal from

another host) and/or vertically (i.e. transovarially from an infected mother to her offspring). Viruses that can be transmitted vertically by their vectors include WNV, DENV and YFV (Mishra 2001, Goddard 2003, Murray 2010, Sall 2010, Buckner 2013). Vertical transmission can allow the interannual persistence of an arbovirus, thus expanding its geographic range to new areas and lengthening the duration of an epidemic (Lambrechts 2009). Viruses that combine vertical transmission with horizontal transmission in the vector population are of interest in evolutionary biology and in public health. *Sigma virus* (*Rhabdoviridae*) is a vertically transmitted, virulent parasite that infects natural populations of *D. melanogaster* worldwide. It is transmitted vertically and biparentally (L'Héritier, 1958; L'Héritier, 1970) and is virulent: infected hosts exhibit decreased fecundity (Fleuriet, 1981). The *Sigma virus – Drosophila melanogaster* model system provides an opportunity to investigate the mechanisms permitting parasite persistence with vertical transmission.

Accurately predicting the spread of arboviruses requires an understanding of how the environmental context can mediate virulence and viral replication – a process which can be modeled mathematically to improve the accuracy of predictions when scaling up to the host population level (Lord 2014). Due to urbanization and agricultural development, some ecosystems have become suitable for arboviruses and their vectors (Weaver 2010). Agricultural development has brought a rapid increase in the availability of carbon (C), nitrogen (N), and phosphorus (P) in freshwater ecosystems – favoring vector species that thrive in nutrient-rich larval environments. Among these vector species are the *Culex pipiens* complex, which includes several important vectors of WNV (Reisen 2013). Ecological Stoichiometry theory predicts that at higher nutrient levels, parasite load should increase (Lafferty 2009); the nature of this relationship is unknown for mosquito vectors where selective pressures on virulence are

expected to minimize the fitness cost of infection. The prediction that viruses are P-limited within their hosts has been supported in an experimental setting, where P was found to increase the prevalence of *Barley yellow dwarf virus* in healthy hosts (Borer 2010). The effects of nutrient enrichment on the abundance of WNV have been investigated at the landscape level in a correlational study (Crowder 2013); however to our knowledge, there is little experimental work on the effects of P on WNV population growth, which we suspect is correlated with virulence. In this dissertation, I experimentally manipulate the concentration of phosphorus in cell culture to determine whether WNV titers would increase under nutrient-enriched scenarios. I then present a mathematical model of virus replication in which I identify areas where phosphorus would have the largest effect on WNV replication.

Recent technological advances have improved our knowledge of the replication process of Flaviviruses; however direct measurement of virus replication in the laboratory can be cost-prohibitive. Mathematical models of the within-host dynamics of virus replication can be useful for predicting virus load, which can affect virulence, transmission rate and rate of molecular evolution. In the case of arboviruses, most mathematical models have focused on transmission dynamics between hosts and vectors. Within-host replication of arboviruses (particularly Flaviviruses) has not been well-characterized mathematically. Several mathematical models of *Hepatitis C virus* (HCV: Flaviviridae) have captured several important aspects of virus replication, generating accurate predictions of within-host dissemination of the virus (Dahari 2007, Kumberger 2016) and of viral entry into host cells (Padmanabhan 2011). Using previous work on mathematical models of HCV replication, I model the replication of WNV in cell culture and generate testable predictions about the spread of the virus within a host. I model the trajectory of a virus population under a set of biologically sound parameter values. As has been

done with HCV, the resulting mathematical model can also be applied in a clinical setting, where there is a growing body of work on the within-host dissemination of Flaviviruses.

Laboratory experiments and mathematical models can facilitate progress towards controlling the spread of arboviruses; however in the absence of field research, the results from these studies cannot be ground-tested and the models cannot be improved. Conducting clinical research in tandem with the development of these models is important. To begin testing our predictions, we initiated an arbovirus surveillance study in Barquisimeto, Venezuela. The focus of this study was to provide information on the ZIKV epidemic in Venezuela, where an immunologically naïve population experienced an epidemic of ZIKV, concurrent with endemic circulation of DENV, CHIKV, YFV and *Mayaro virus* (MAYV). Venezuela is situated in an area of high circulation of arboviruses (Hotez 2017). The effects of co-infection and immunological status can thus be investigated *via* clinical research on patients reporting symptoms of febrile illness. In the final section of this dissertation, I present a case study from an epidemiological study in which we identify virus loads and transmission mode of ZIKV in an immunologically naïve population.

The establishment of an arbovirus involves processes that operate at multiple scales of biological organization (e.g. physiological, ecological and evolutionary). A multidisciplinary approach that combines field surveillance, laboratory experiments and mathematical models can provide effective tools for linking these scales and generating testable hypotheses for future work (Lloyd-Smith 2009, Lord 2014). In this dissertation, I combine field surveys, laboratory experiments and mathematical models to address several aspects of the establishment of arboviruses. Specifically, I investigate 1) how transmission mode (vertical vs. horizontal transmission) can affect the persistence of a virulent parasite in the *Sigma virus – Drosophila*

melanogaster model system; 2) how non-living environmental factors (specifically phosphorus enrichment) can affect the replication of WNV; 3) how mathematical models can improve our understanding of the replication cycle of clinically important RNA viruses; and 4) how laboratory methods and field studies can be designed to detect emerging viruses in resource-limited settings – specifically in Venezuela during the ZIKV epidemic in 2016.

CHAPTER 2
Drosophila melanogaster AND SIGMA VIRUS: A MODEL SYSTEM FOR UNDERSTANDING THE PERSISTENCE OF VERTICALLY TRANSMITTED ARBOVIRUSES

The prevalence and persistence of a parasite are constrained by the host's population density (Bjornstad et al. 2002), life history and genotype, by the transmission mechanism of the parasite, and by the impact of the parasite upon its host. Virulence – the reduction of host fitness by a parasite – may impose a cost on the parasite as well as the host, if decreased host lifespan or fecundity results in decreased rates of parasite transmission. However, increased virulence may also benefit the parasite, as virulence is often closely linked to the diversion of host resources for parasite reproduction. The costs and benefits of virulence to the parasite are thus expected to balance each other to some extent, giving rise to an optimal (for the parasite) intermediate level of virulence (*i.e*., the tradeoff theory for the evolution of virulence) (Ebert 1999; Combes 2001; Alizon & van Baalen, 2005). There are other factors, of course, that can influence virulence (Ebert & Bull, 2003), but in some systems the nature of transmission makes costs for the host likely to be costs for the parasite as well. This is inevitable when transmission is vertical across host generations.

Virulence is particularly costly to parasites that are transmitted vertically (from parents to offspring) because parasite fitness is so closely tied to host fitness: hosts that die before reproduction doom their parasites as well, and if parasite reproduction involves passage through host eggs, reduced host fecundity also reduces parasite fitness. The persistence of vertically transmitted parasites that remain virulent despite their mode of transmission thus presents both an ecological puzzle (how does the parasite persist?) and an evolutionary puzzle (why doesn't selection act to reduce virulence, if it is costly to the parasite, too?). Observing such a system often leads to a working hypothesis of the existence of some form of cryptic horizontal

transmission (*i.e.*, transmission within generations rather than from parent to offspring (Mangin et al. 1995). Parasites that combine vertical transmission with horizontal transmission, involving both within- and among-species transmission, are not uncommon. Examples of viruses that include both vertical transmission within a dipteran population and horizontal transmission between dipteran vectors and human hosts include West Nile and yellow fever viruses (Mishra & Mourya, 2001; Goddard et al. 2003; Murray et al. 2010; Sall et al. 2010).

Another factor that can affect persistence is diversity in the modes of vertical transmission. In sexual host species, vertical transmission can be uniparental (typically maternal) or biparental (either parent can infect the offspring). A virulent parasite cannot persist by uniparental transmission alone; at least some horizontal transmission is required. In contrast, biparental inheritance permits persistence of virulent parasites with no horizontal transmission, at least if transmission efficiency is high relative to the cost of infection (Fine, 1975), and moreover changes the selective pressures on both the host and the parasite. Biparentally transmitted parasites have epidemiological and evolutionary similarities to horizontally transmitted parasites (Fine, 1975). Systems with biparental transmission may provide an unusual opportunity to understand the ecology and evolution of virulence, because transmission to new host lineages occurs *via* sexual reproduction, which can be easier to document and to experimentally manipulate in these systems (which necessarily are structured by mating pairs) than in many modes of horizontal transmission.

The sigma virus – *Drosophila melanogaster* model system provides an ideal opportunity to investigate the mechanisms permitting parasite persistence without horizontal transmission. Sigma virus (Rhabdoviridae) is a vertically transmitted, virulent parasite that infects natural populations of *D. melanogaster* worldwide (reviewed in Fleuriet, 1996). It has long been known

to be transmitted biparentally (L'Héritier, 1958; L'Héritier, 1970). Sigma is virulent: infected hosts express a variety of symptoms consistent with lowered fitness, including a decrease in fecundity (Fleuriet, 1981). This is the kind of fitness cost in the host that also imposes a potential fitness cost on the parasite. Sigma virus infections have been observed in several other species of *Drosophila* (e.g., *D. affinis* and *D. Athabasca*) (Williamson, 1961; Félix et al. 1971b; Longdon et al. 2010), suggesting that this is a widespread host-parasite syndrome.

Our specific goal in this study is to ascertain if transmission efficiency and virulence as estimated from field and laboratory studies are consistent, even broadly, with levels of prevalence observed in nature. To achieve this goal, we develop a dynamic, deterministic, discrete-generation model that incorporates sex-specific transmission efficiency and cost of infection with respect to fecundity for projecting disease prevalence across time. Using data from a natural population of flies, we estimate prevalence, track transmission efficiency across generations and lineages, and also quantify the effect of sigma infection on female fecundity (a key aspect of virulence). We use the results of these lab studies to parameterize the model, and then compare the equilibrium prevalence predicted by the model to the prevalence measured in our field samples. In the discussion, we sketch future extensions of the modeling framework that may be needed to account for some of the empirical patterns we observed in the lab studies.

Modeling the Dynamics of *Sigma virus*

Our model is broadly based on models presented by L'Heritier (1970) and Yampolsky et al. (1999), but differs from the former in that we do not distinguish among hosts differing in level of infection (what L'Heritier refers to as the stability of the infection), and from the latter in that we incorporate costs to female flies of being infected, and also permit a broader range of transmission efficiency when both members of a mating pair are infected. Given the current prevalence (*pt*, the fraction of flies that are infected, which is assumed to be independent of sex),

the prevalence in the next generation (pt+1) is the ratio of the *per capita* proportion of infected offspring to the *per capita* production of all offspring. Infected offspring are produced in three ways: 1) an infected female with fecundity *ni* and transmission efficiency *eF* mates with an uninfected male; 2) an uninfected female with fecundity *nu* mates with an infected male with transmission efficiency *eM*; or 3) two infected flies mate with fecundity *ni* and transmission efficiency *eB* (the probability that an offspring of two infected parents is infected). We assume that infection affects only female fecundity, resulting in an asymmetry in the equations below with respect to male and female transmission parameters. We further assume that there is no sex-specific effect of infection on survivorship, so infected, fertilized eggs have an equal chance of entering the mating pool, regardless of their sex. We also assume that mating is random with respect to infection status: therefore, the probability that a randomly chosen mating pair consists of an infected and an uninfected fly is $pt(1 - pt)$, and the probability of both parents being infected is pt. The *per capita* number of infected eggs is the sum of products of mating probabilities, fecundities and transmission efficiencies for events producing infected offspring, which is [$pt(1 - pt)(nieF + nueM)$+pt 2$nieB$]. The *per capita* number of eggs produced is the weighted average of the uninfected and infected fecundities [(1-pt)nu +$ptni$]. Taking the ratio of these quantities gives the Equation 2-1

$$p_{t+1} = \frac{p_t(1-p_t)(n_i e_F + n_u e_M) + p_t^2 n_i e_B}{(1-p_t)n_u + p_t n_i} = \frac{p_t(1-p_t)(qe_F + e_M) + p_t^2 q e_B}{1 - p_t + p_t q} \qquad (2\text{-}1)$$

where $q = n_I/n_U$ is the fecundity of infected relative to uninfected females, which could include differential oviposition rate and even egg viability (as long as egg viability depends on infection of the female, not the eggs). As q decreases, the cost of the virus to the host (virulence) increases. We analyze the properties of this model in the Results section. We then relate this

model to data, including estimates of prevalence, sex-specific transmission efficiency, and the impact of infection on female fecundity.

Methods

Our focal population for the study consisted of a population of *D. melanogaster* in north-central Georgia, USA. To measure the prevalence of sigma virus, we sampled natural populations of *D. melanogaster* from six sites along US Hwy. 129/441 (Table 2-1).

Table 2-1. Location of collection sites. All sites are along U.S. Highway 441/129 between Eatonton and Athens, GA. Distance is indicated in miles along the highway from the southernmost site (site 1).

Site ID	Distance (mi)	Coordinates
6	50	33° 94.671' N
5	35	33° 49.463' N
4	23	33° 46.528' N
3	22	33° 46.264' N
2	20	33° 44.447' N
1	0	33° 24.578' N

We collected five times during the summer of 2009: June 12, June 24, July 10, July 24 and September 18. Twenty-four hours before sampling, we placed 3 baits containing fruit and yeast at each site to attract *D. melanogaster*. We then swept for all visible flies using *Drosophila* fly nets (Bioquip®). We transferred the animals to plastic shell vials containing standard molasses- cornmeal medium, and brought them to the University of Florida in Gainesville. All animals were assigned to individual vials in the laboratory within 72 hours of the collection time.

Because exposure to CO_2 is lethal to flies that are infected with sigma virus (L'Héritier & Teissier, 1945), animals were anesthetized using cold treatment, a standard alternative to the more common procedure of CO_2 anesthesia. We first placed the insects in empty vials in ice for up to 5 minutes. Once the insects stopped moving, we transferred them to custom-made metal blocks which had been chilled for >1 hour at 0°C and covered with moist KimWipes. We discarded all species except *D. melanogaster*, which we placed individually in *Drosophila* plastic vials with standard molasses-cornmeal medium.

CO_2 Assay for Sigma Virus Infection

Infection status was determined by CO_2 assay. Each fly to be assayed was placed in an empty vial, which was flooded with CO_2 for 5 minutes, and then returned to ambient oxygen and CO_2 levels for 15 minutes. Flies that returned to normal activity levels (walking and flying) were scored as uninfected; flies that were either dead or paralyzed (unable to walk or fly but still moving) after CO_2 exposure were scored as infected. Because the assay kills or paralyzes infected flies, flies were allowed to reproduce before they were assayed for infection.

Transmission Assays

Field-collected adults will hereafter be referred to as the parental (*P*) generation. By holding these flies in individual vials for five days prior to CO_2 assay (which is lethal to infected animals), we were able to rear their progeny (the F_1), assay the F_1 for sigma virus infection, and thus estimate transmission efficiency (Figure 2-1). We assayed the F_1 by CO_2 as described above to determine their infection status, 10-12 days after establishment of the vials. Transmission was estimated as the fraction of F_1 offspring produced by an infected parent that were infected (calculated separately for male and female parents).

Females captured from the field are usually inseminated, and thus can produce viable offspring without mating in the laboratory. We therefore placed the field-collected females individually in vials and allowed them to oviposit for five days. The infection status of the sires of these $F1$ was thus unknown. To determine rates of transmission by field-collected males, we crossed each male with two uninfected virgin females from the effectively isogenic 58 stock (Wayne et al. 2007), and left them in the vial together for five days. $F1$ progeny were collected on day 14 after the vial was established. We determined the single-generation transmission efficiency of males and of females obtained from three collection trips: June 24 (trip 2), July 10 (trip 3), and July 24 (trip 4), 2009.

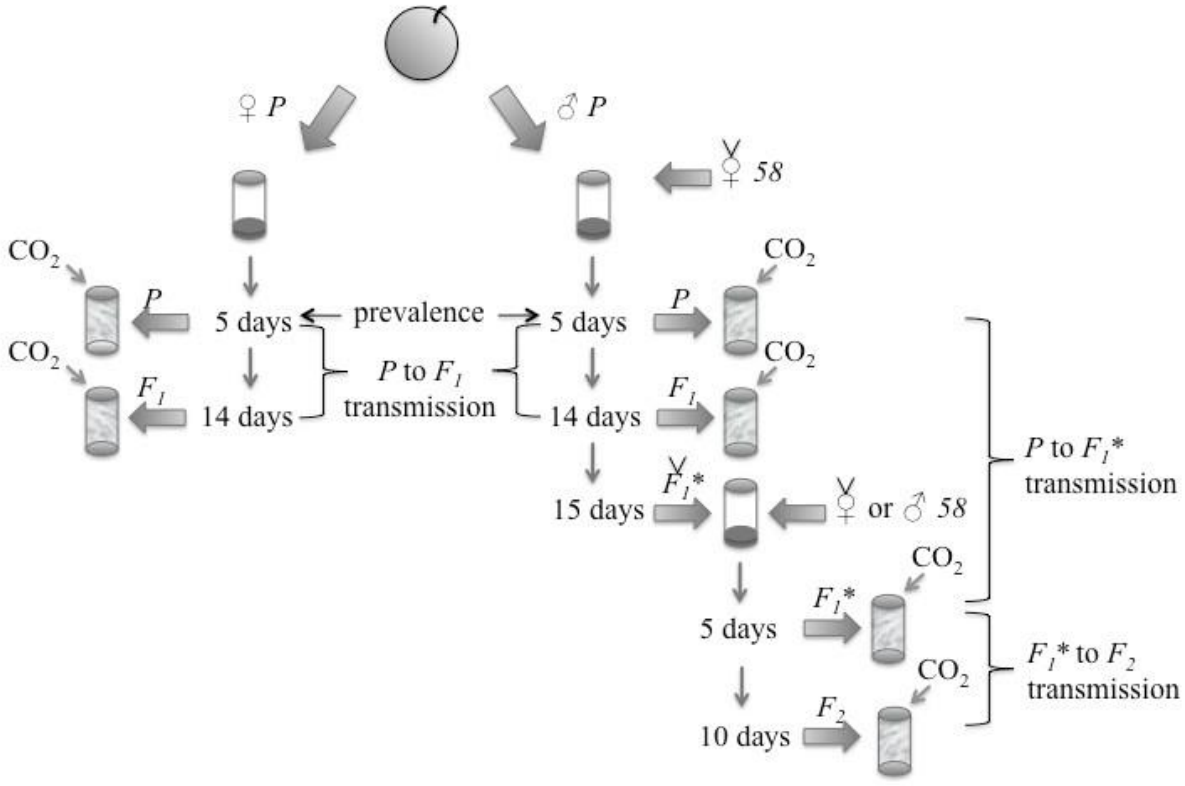

Figure 2-1. Procedure for measuring prevalence and transmission. This diagram shows how prevalence and transmission were measured, in females (left side) and males (right side). Heavy arrows denote movement of animals; thin arrows denote passage of

time. P denotes the generation captured from peach stands (i.e., from the field). The F1 are the progeny of the field-caught animals and the F2 are their grand-progeny. Prevalence and P to F1 transmission were measured for both female and male P animals. The progeny of these 11 isomale lines (all of which were from trip 4) are denoted as F1*. Second, P to F1* includes only virgin F1* animals (as indicated by the V) from day 15 (in contrast to P to F1 transmission efficiency, which included non-virgin progeny from days 10-14)

Our statistical model tests for the effects of sex and trip on transmission efficiency, using the standard linear modeling function (lm) in R (R Development Core Team 2008). We treated trip as a factor and first determined the statistical significance of the interaction between sex and trip. We then reduced the model by eliminating the non-significant interaction between sex and trip ($P = 0.237$) to keep an additive model of the effects of sex and trip. We checked our data and the residuals graphically for deviations from the assumptions of linear models (normality, homogeneity of variance: plot.lm function in R: R Development Core Team 2008), and observed no large deviations.

Multigeneration Patrilineal Transmission

As noted in the introduction, given the complete lack of evidence for any horizontal transmission, biparental transmission is required for persistence of the sigma virus in natural populations. To further characterize biparental transmission, we monitored patrilineal transmission efficiency across three generations originally sired by infected male *P* flies from the July 24th trip (trip 4; Figure 2-1). A subset of eleven infected males assayed for transmission as described above were used to create eleven independent "isomale" lines. After the original transmission assay using $F1$ progeny collected on day 14, additional unmated progeny (denoted as $F1$* virgins) were collected twelve hours later (10-13 $F1$* virgins per vial). We next set up single pair matings by pairing each $F1$* fly with a single uninfected virgin of the opposite sex from the effectively isogenic *58* stock. Five days after establishment of the $F1$* vials, the parents

were removed and assayed for infection using the CO_2 assay. Only $F1^*$ vials of infected parents were retained. The percentage of $F1^*$ flies infected is referred to as the *P* to $F1^*$ transmission efficiency. When the offspring (the $F2$) flies eclosed 12-14 days later, we determined the infection status of 10 haphazardly chosen $F2$ flies from each vial using CO_2 assay. The sexes of the $F2$ progeny were not recorded. The percent infected $F2$ offspring is referred to as the transmission efficiency from the $F1^*$ to the $F2$ generation. We analyzed the data from these experiments using three separate paired *t*-tests; all comparisons were made within each of the 11 lineages. We first determined whether the probability of acquiring sigma virus infection from the *P* males was equal for both male and female $F1$ flies. We then compared the transmission efficiency ($F1^*$ to $F2$) from infected $F1^*$ female to that of infected $F1^*$ male flies, to test for sex-specific differences in transmission efficiency in animals who acquired infection from the sire (male parent). We finally compared the transmission efficiency of *P* males to that of their male $F1^*$ progeny, to estimate changes in patrilineal efficiency from one generation to the next.

Effect of *Sigma Virus* on Female Fecundity

With vertical transmission, impairment of female fecundity hampers the persistence of the parasite. Accordingly we measured the effect of sigma virus on female fecundity (number of eggs per female). We compared 4 infected isofemale lines to 4 uninfected isofemale lines of *D.melanogaster* collected near Athens, GA in the summer of 2007. Isofemale lines are created by placing a single, inseminated wild-caught female in a vial and propagating her offspring *en masse*. Thus, these lines represent a small random sample from the population, and are expected to be genetically distinct from one another. We conducted four blocks of measurements, each with four replicate bottles (total: 4 lines x 2 infection statuses x 4 blocks x 4 replicate vials/block = 128 vials). For two generations prior to assay, flies were propagated in vials set up at constant

density (5 females + 5 uninfected males per vial), ovipositing for five days on standard cornmeal-molasses medium. For the assay, individual female flies, four days post-eclosion, were placed in inverted milk bottles over small Petri dishes containing cornmeal-molasses food. After six hours, we counted the number of eggs that were laid by each female. While performance of lines within treatments was consistent across blocks, the mean of treatment groups varied between blocks, precluding a traditional ANOVA treatment.

Relating the Model to Experiments

We parameterized the prevalence model (Equation 1) with the fecundities and transmission efficiency measured in the lab to predict sigma prevalence at the non-zero equilibrium. To obtain point estimates and confidence intervals for transmission efficiencies, we used maximum likelihood estimation (bbmle: Tools for general maximum likelihood estimation. R package version 0.9.5.1; http://CRAN.R-project.org/package=bbmle (Bolker, 2008) to fit beta distributions (parameterized in terms of mean and variance parameters; Morris, 1997) to the proportions of offspring infected from crosses with either an infected female (for eF) or male (for eM). We based our model parameters on the estimates and confidence intervals (CIs) for the means of these distributions. We used the same method to derive a point estimate and confidence intervals for the observed prevalence. We similarly used maximum likelihood, but based on a negative binomial distribution, to derive point estimates and CIs for the fecundity of infected and uninfected flies. We calculated the expected prevalence and rate of increase at low prevalence by substituting the mean observed parameter values in the expression for the equilibrium prevalence. We used nonparametric bootstrapping ($n = 10^7$) using all observed values of fecundity and transmission efficiency to find confidence intervals on these quantities.

Results

Transmission Efficiency

We measured transmission efficiency (proportion of offspring which were infected) for males and females. Both sexes transmitted the virus, but with different efficacy. Males transmitted sigma virus to a mean of 51% (± 8% std. error) of their offspring, while females transmitted sigma virus to 95% (± 5% std. error) of their offspring (Table 2-2).

Table 2-2. ANOVA results for single-generation transmission efficiency. There was a statistically significant effect of sex on the transmission efficiency of sigma virus (females transmitted at a higher rate than males).

Source	Df	Sum Sq	Mean Sq	*P*
Sex	1	1.507	1.507	< 0.0001
Trip	2	0.136	0.068	0.0081
Error	37	0.456	0.012	

Multigeneration, patrilineal propagation of sigma virus was possible for multiple generations in the lab, using "isomale" lines (each of which was propagated from an infected sire obtained in the field (*P* generation) mated with a single virgin female from the effectively isogenic laboratory stock *58*). All 11 *P* generation males transmitted sigma virus to some offspring(each representing new female lineages; Figure 1-3, left panel). Sons and daughters ($F1^*$ flies) were equally likely to become infected with sigma virus when the sire was infected (paired *t* test; $P = 0.79$). Intriguingly, daughters of infected males had a higher transmission efficiency than did sons ($F1^*$ to $F2$ transmission efficiency; Figure 1-3, middle panel; paired *t* test, $P = 0.032$). Moreover, transmission efficiency from sire to offspring was significantly lower in the $F1^*$ to $F2$ generation than in the *P* to $F1^*$ generation (Figure 1-3, right panel; paired *t* test, $P = 1.149 \times 10^{-6}$).

Prevalence

Prevalence was estimated five times in the summer of 2009, for flies collected from six sites (data presented in Table 2-3). The average prevalence of sigma virus was 28% (Figure 1-2). Prevalence did not differ significantly by sex, by site, or by trip; nor were any of the interaction terms significant (Table 2-4). However, prevalence did vary among collection trips, ranging from zero infected flies found (3 out of the 20 samples that yielded at least one fly of each sex; Table 2-3), to 71% prevalence (July 24, site 4; Table 2-3). There are no obvious trends predicting prevalence (Figure 1-2).

Table 2-3. Virus prevalence and number of flies per collection. Each site is labeled according to its distance from the southernmost site. We measured prevalence as the proportion of flies infected with sigma virus for each date and site combination. Dashes indicate that the number of flies of at least one sex was zero.

Date	Distance (mi)	Uninfected F	Infected F	Uninfected M	Infected M	Prevalence
12-Jun	*0*	13	2	14	3	0.16
	20	6	0	5	3	0.21
	22	0	0	1	1	--
	23	0	0	1	0	--
	35	14	4	25	4	0.17
	50	13	0	8	0	0
24-Jun	*0*	3	0	0	3	0.5
	20	0	1	1	1	0.67
	22	0	0	0	0	--
	23	2	0	2	0	0
	35	0	0	0	0	--
	50	2	3	4	2	0.46
10-Jul	*0*	3	3	6	0	0.25
	20	2	1	3	0	0.17
	22	1	1	2	0	0.25
	23	2	0	4	0	0
	35	0	0	0	0	--
	50	3	5	4	2	0.5
24-Jul	*0*	6	3	11	2	0.23
	20	8	3	2	1	0.29
	22	0	0	0	0	--
	23	0	2	2	3	0.71
	35	0	0	0	0	--
	50	4	0	13	5	0.23
18-Sep	*0*	0	0	0	0	--
	20	7	1	2	0	0.1
	22	1	0	4	3	0.38
	23	1	0	0	0	--
	35	0	0	0	0	--
	50	17	14	37	21	0.4

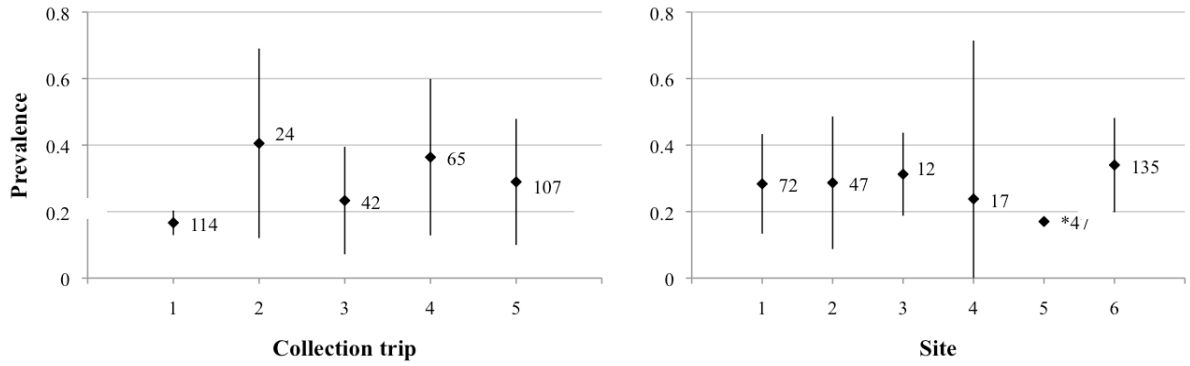

Figure 2-2. Prevalence of sigma virus in North-central Georgia. The proportion of D. melanogaster that are infected with sigma virus is shown (± 2 SE). Variance in prevalence at the 35-mile site (* point without error bars) could not be estimated, because we collected *D. melanogaster* during only one of the collection trips to this site. Sample size (number of flies) is indicated next to each point. The mean proportion of flies infected with sigma virus was 0.28 ± 0.1

Table 2-4. ANOVA results for the prevalence of sigma virus in the field. There were no statistically significant effects of date, site, or sex on the prevalence of sigma virus, nor any significant interaction terms

Source	Df	Sum Sq	Mean Sq	*P*
Trip	4	2.71	0.678	0.17
Site	5	0.38	0.075	0.95
Sex	1	0.23	0.228	0.43
Trip x Site	13	4.62	0.355	0.48
Trip x Sex	4	0.99	0.247	0.6
Site x	5	0.31	0.062	0.96
Residuals	10	3.42	0.342	

Virulence and Cost to Fecundity

Four infected and four uninfected isofemale lines were scored for fecundity. Females from the infected lines laid a mean of 115 eggs each (± 58; standard error of the mean), while females from the uninfected lines laid a mean of 169 eggs each (± 85; standard error of the mean). The performance of individual lines was consistent across the four assay blocks.

Generally speaking, lines that were infected had lower fecundity than uninfected lines (Figure 1-3). However, in one out four blocks, infected and uninfected lines performed similarly.

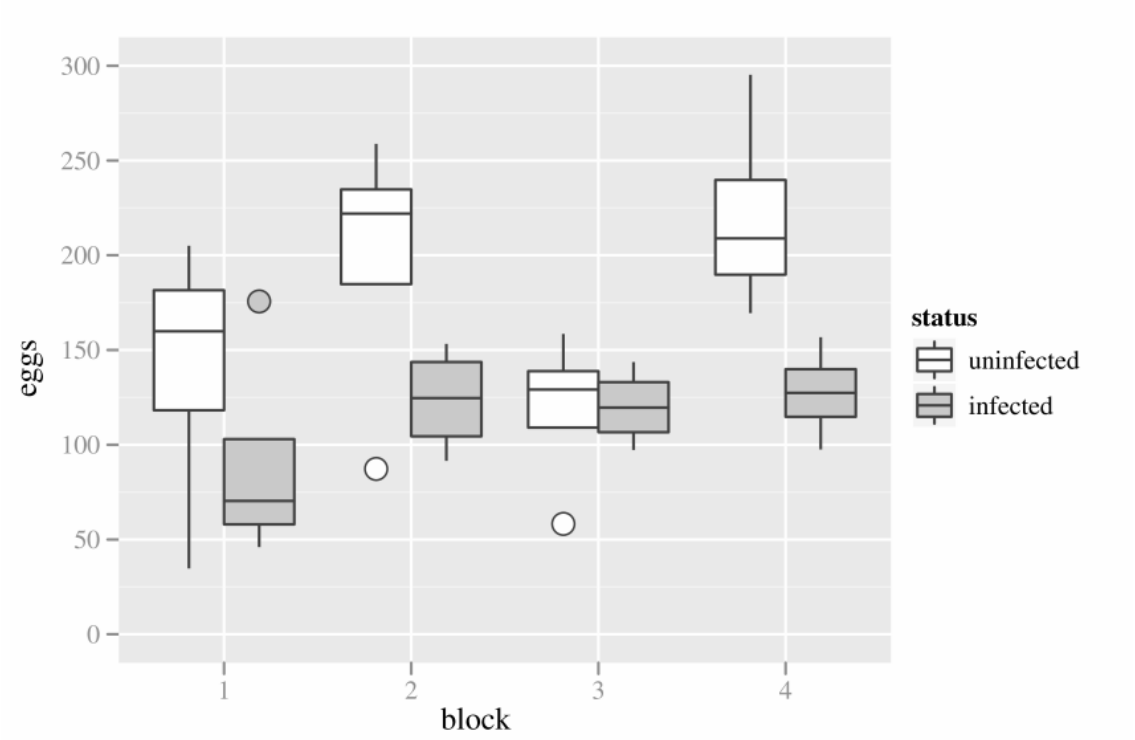

Figure 2-3. Effect of infection status on fecundity. Boxes represent the means of lines within treatments (i.e., uninfected, white boxes; vs. infected, gray boxes) for each of the four blocks. Error bars represent two standard deviations from the mean of each group of four lines. Circles represent outlier lines within treatments (i.e., lines more than 1.5 times the group interquartile range), and are shaded to indicate infection status as described above. Fecundity is generally higher in uninfected lines than in infected lines, except in the third replicate.

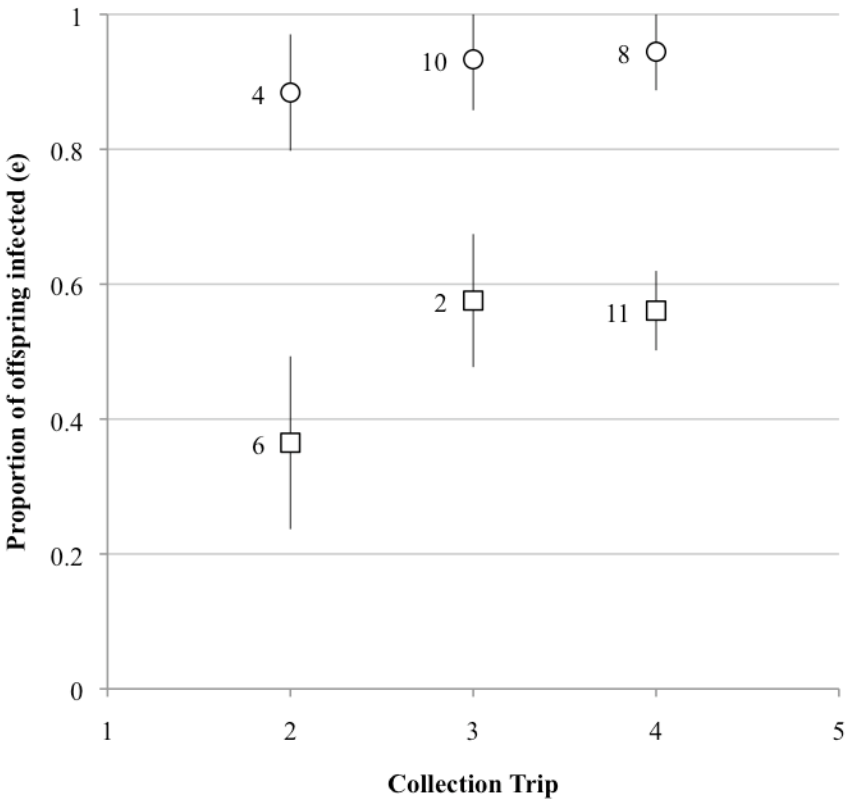

Figure 2-4. Transmission efficiency of sigma virus (single-generation). Mean transmission efficiency by females (circles) and males (squares), calculated from the first ten F1 offspring to eclose (± 2 SE). Sample sizes (number of flies) are indicated next to each point. Flies from collection trip 1 were not assayed for transmission efficiency; while transmission efficiency wasassayed from collection trip 5, a different protocol was used such that the data were not comparable.

Interestingly, although it was previously been stated that the sons of infected males do not transmit the virus (L'Héritier, 1970; Fleuriet, 1981), we have demonstrated that multiple generations of patrilineal transmission are possible, at least for virus and flies from the Athens, GA population. However, transmission frequency is lower from the second to third generation of patrilineal transmission than from the first to the second (Figure 2-5).

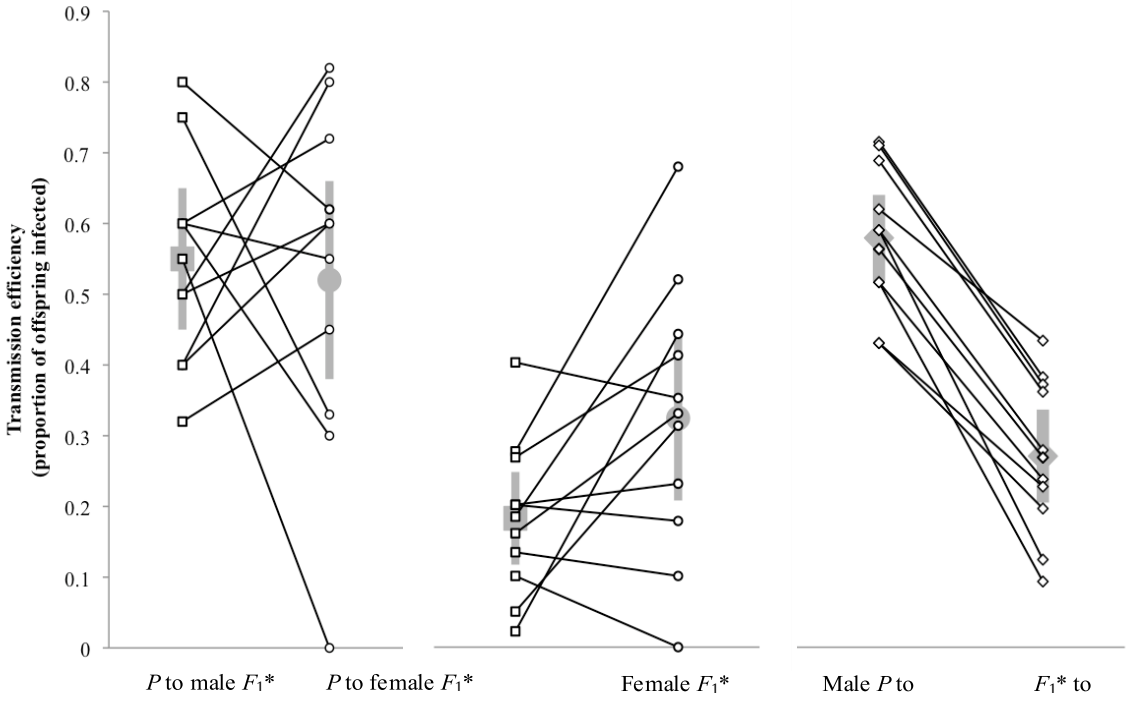

Figure 2-5. Patrilineal transmission of sigma virus. Transmission efficiency (the proportion of the first 10 offspring that were infected) is illustrated on the Y-axis, which has the same range in all panels. Thin black lines correspond to each of the 11 isomale lineages. The grand means (± 2 SE) of the lines are shown in heavy grey lines. The left panel represents transmission efficiency between the *P* and *F*1* generations, testing the hypothesis that patrilineal transmission is equal in sons (open squares) and daughters (open circles; $P = 0.79$). The middle panel compares transmission efficiency from the *F*1* to the *F*2, specifically between sons (open squares) and daughters (open circles) of infected sires from the field; transmission is higher from *F*1* daughters than *F*1* sons ($P = 0.032$). Finally, the right panel represents the decrease in transmission efficiency (open diamonds: combining male and female offspring) from the first to the second generation (i.e., *P* to *F*1* relative to *F*1* to *F*2; $P < 0.0001$).

A more complex model than (1) above would be needed to encompass this intriguing transgenerational effect on transmission, as well as to incorporate the distinction among classes of hosts with different patterns of within-host dynamics first explored by L'Heritier (1970). A consideration of distinct patterns of within-host dynamics may be needed to fully explain our results. We also have demonstrated that infection acquired solely from the sire persists for at least two generations in the lab, although transmission efficiencies decline with each generation. The

persistence of paternally-acquired virus is particularly important because, as reiterated by our model results and previously demonstrated by others, biparental inheritance is required for persistence of vertically transmitted parasites (Fine, 1975). One biological consequence of such male transmission is that given occasional interspecific hybridization, the virus could be transmitted across species boundaries. As noted above, sigma virus is currently known to infect several species of *Drosophila* (Williamson, 1961; Félix et al. 1971b; Longdon et al. 2010). It would be interesting to have a fuller understanding of the phylogenetic scope of sigma virus among closely related species of flies, coupled with a deeper understanding of patterns of genetic variation in the virus within single host species. Future studies will incorporate population-genetic components that include genetic variation of both the host and the parasite. Together with the ecological factors sketched above, genetic differences could play a strong role in explaining differences among sites in sigma virus prevalence. For example, viral variation that causes detectable differences in transmission and/or infectivity is well known (Goldstein, 1949; Brun & Plus, 1980; Wilfert & Jiggins, 2010a). Host genetic variation for male transmission and for resistance is also well documented (L'Héritier, 1970; Gay, 1978; Brun & Plus, 1980; Fleuriet,1996; Wayne et al. 1996; Bangham et al. 2007; Bangham et al. 2008; Carpenter et al. 2009; Wilfert & Jiggins, 2010b). However, data on allele frequencies in virus and host, as well as potential host-parasite interactions (or lack thereof; Wilfert & Jiggins, 2010b), are required to make meaningful progress in this direction.

Discussion

Our point estimate for prevalence based on lab estimates of sex-specific transmission and cost of infection on fecundity is consistent with prevalences observed in the field; however, lab-estimated parameters also produce very wide confidence intervals, and the equilibrial prevalence they predict tends to exceed observed field values (Figure 2-6)

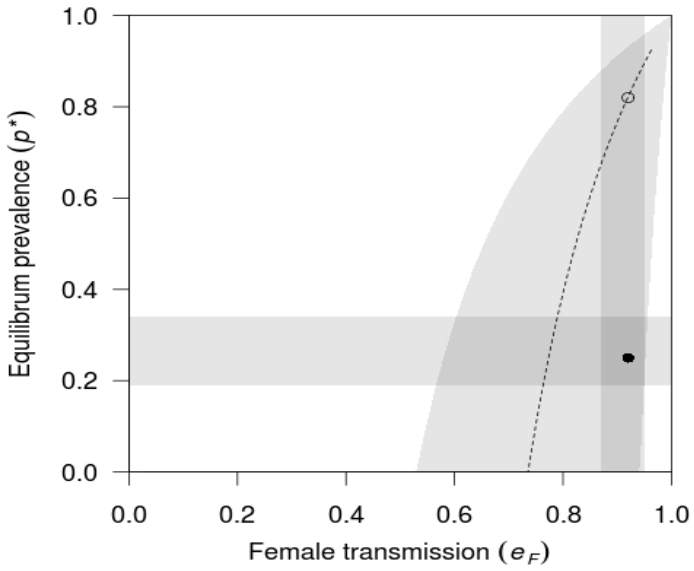

Figure 2-6. Equilibrium prevalence of *Sigma virus* as a function of female transmission efficiency and male transmission efficiency. The open circle is the prevalence predicted using the point estimates of the parameters and equations. The filled circle represents the observed mean prevalence and mean female transmission efficiency; error bars represent 95% binomial confidence intervals at the observed prevalence. The dashed curve shows the expected prevalence as a function of female transmission, given that male transmission is equal to its point estimate (0.5).

Regardless, the overlap suggests that our model provides a sensible springboard for more detailed investigations of virulence and transmission in the sigma virus-*Drosophila* system, including a wider range of known and suspected biological factors. Our estimates of prevalence and transmission efficiency were obtained from the same population of flies within a single season, and our estimates of virulence were obtained from the same population (albeit two years earlier). We found that sigma infects a mean of 28% of *D.melanogaster* individuals in north-central Georgia (approximate latitude 33.9°N), with no differences in prevalence between males and females. The prevalence of sigma virus in 2009 (when flies were collected for our lab study) was higher than in 2005, when it infected only 6.2% of the population of *D. melanogaster* in Athens, GA (Carpenter et al. 2007); or in 2006, when it infected 7% of the population (Wayne

unpublished data). Thus, prevalence in these natural populations varies greatly from season to season. While it is possible that prevalence in the 2009 season was anomalous, note that transmission efficiencies were obtained from the same population for the same season (though virulence estimates are from lines collected in 2007), so the data are at least self-consistent. Our estimate of virulence (32%), while high, is not grossly dissimilar from previous estimates of virulence in terms of egg to adult viability. For unstabilized females, the decrease in fecundity has been estimated at 19% (± 4.6%), and for stabilized females, at 10% (± 2.4%; Fleuriet, 1981). It is interesting to place our field estimates of prevalence into a broader geographical context. The prevalence of sigma virus in our study area, which is among the southernmost sites studied to date (33.9°N), is also among the highest yet recorded, at 25%; though again prevalence varies among years (6.2 % in 2005; Carpenter et al. 2007); 7% in 2006 (Wayne, unpublished data). In Athens, Greece (37.9°N), sigma was found in 14.9% of the population (Carpenter et al. 2007); in Galicia, Spain (42.66°N), prevalence was 4.3% (Carpenter et al. 2007); in Languedoc, France (43.7°N), prevalence ranged from 10-20% (Fleuriet, 1976; Fleuriet, 1980; Fleuriet, 1996) ; in Ithaca, NY (47.4°N), prevalence was a mere 1.7% (Yampolsky et al. 1999); and finally in Essex, UK (51.79°N), prevalence was 7.0%, though prevalence was zero in nearby Kent, UK (Carpenter et al. 2007). Latitude is of course an imperfect proxy for climatic variables that presumably can exert an influence on prevalence, but inspecting this suite of studies suggests to us the existence of a latitudinal or climatic gradient in prevalence of sigma virus. (Note that Galicia is on average considerably wetter and cooler than both Languedoc and lowland Greece.). One published outlier to this trend comes from Clermont, FL (Apshawa Road; 28.61°N), the southernmost site, where prevalence was estimated at 1.5% (Carpenter et al. 2007). There are reasons to believe that prevalence may be low for several reasons distinct to that study. First, it was estimated early in

the season (March 2005); second, *D. melanogaster* is locally rare in the area; and third, the viral isolate was quite distinct from all other samples sequenced (Carpenter et al. 2007; Longdon et al. 2010), and so might well have distinct epidemiological properties. Our analysis of the model assumed that a population had reached equilibrium, and that fitness costs of parasitism are fixed. Natural populations are likely to be strongly disequilibrial. Fly populations are likely to fluctuate greatly in numbers, in response to variation in climate, fluctuations in resource availability, and other factors, and may go extinct and become replenished by re-colonization. If sigma virus is lost by chance from a population at low numbers, when it recolonizes there will be a lag before it reaches equilibrium, and during this lag prevalence will be less than the local equilibrium. We measured fitness costs of parasitism to female fecundity in the lab, but it is plausible that additional costs could be incurred in natural conditions when females are exposed to a wide range of stressors. This too would tend to depress viral prevalence. For example, variation in prevalence in Mexico City might be explained by decreased overwintering survival of infected relative to uninfected flies and thus reduced frequency of infection of founders of the following spring population (Félix et al. 1971a), combined with low dispersal among populations. Likewise, male mating success might be more strongly affected by infection in the field than in the lab, and this could lead to low infection in sparse populations (as in the Clermont, FL population noted above). We note also that if there is spatial or temporal variation in R (or q), and local populations equilibrate in prevalence rapidly in response to such variation, then by Jensen's inequality from the concave-down shape of (5) where $R > 1$, prevalence averaged across sites will be less than the prevalence estimated from averaged values of the parameters (Inouye, 2005). Without empirical estimates for his model parameters, L'Heritier (1970) sensibly examined a broad range of plausible values. He did, however, include "stability" in his model, where stability

is defined as a persistent level of infection within female hosts, including near-certainty of transmission to offspring. In contrast, we chose to model sex-specific transmission efficiencies and associated errors, as informed by our empirical data, rather than including stabilization status *per se*. Interestingly, we rarely observed female transmission efficiency of 100%. Similar to the models of L'Heritier (1970) and Yampolsky et al. (1999), our model shows that if transmission by one parent is less than 100%, at least some transmission by the other parent is required for persistence (eq. [3]). Our estimates of transmission efficiency are similar to those of Yampolsky et al. (1999), who inferred that the transmission efficiency for the two sexes must be around 0.67 based on the rate of the spread of infection within their experimental populations. Our estimates range from just over 0.5 (for males) to 0.95 (for females), and so bracket this value. As previously noted (L'Héritier, 1970), virus acquired solely from the sire is transmitted at lower rates by daughters than is virus acquired from the dam (Figure 2-5).

CHAPTER 3
EFFECTS OF PHOSPHORUS ON THE REPLICATION OF *WEST NILE VIRUS* IN CELL CULTURE

West Nile virus is a positive-sense RNA virus belonging to the genus *Flavivirus* of the family *Flaviviridae*, which contains more than 100 species of viruses. Clinically important members of this family include vector-borne viruses and others which are transmitted through direct contact. such as *Yellow Fever virus* (YFV), *Dengue virus* (DENV), *Japanese Encephalitis virus* (JEV) and *Zika virus* (ZIKV) are transmitted by mosquitos. Clinical symptoms of infection with these viruses include febrile illness and in some cases neurological disease (Knipe 2001).

WNV is the most widespread arbovirus in the world; it is transmitted by several species of mosquitos in North America (Turell 2005) and it has been detected in least 100 species of wild and domestic animals (Root 2013). In a recent study, Crowder et al (2013) investigated the relative effects of rainfall, host abundance and land use type on the prevalence of West Nile Virus. They found a strong positive correlation between land use type and infection rates of humans and horses: interestingly, land use type was a better predictor of WNV abundance than were the other factors, even when controlling for host density.

Nutrient enrichment brings an increase in nitrogen, phosphorus and other macronutrients. The concentration of phosphorus [P] correlates positively with the concentration of RNA in tissues and with per-unit mass metabolic demands (Sterner 2002). Phosphate is an abundant component of agricultural fertilizers and is a rate-limiting nutrient in many ecosystems: a small addition of P relative to nitrogen leads to large increases in growth rate. Given the stoichiometry of cells and viruses and the high per-unit-mass concentration of phosphorus in viruses, it is reasonable to expect that virus replication could be phosphorus-limited. The effects of the cell's nutritional environment on virus replication are poorly understood; rate-limiting nutrients such as phosphorus can affect the assembly and maturation of virus particles within a

host. Phosphorus is important for intracellular regulation of pH, thus affecting the maturation process of virus particles. Investigating how phosphorus might mediate the strength of the relationship between cells and virus could shed light on how nutrient enrichment might affect vector competence.

Methods

All experiments in this chapter were conducted in the Biosafety Level 3 (BSL-3) laboratory at the Florida Medical Entomology Laboratories at the University of Florida campus in Vero Beach, FL following established procedures. Preparation and filter-sterilization of cell culture media was conducted in the Biosafety Level 2 (BSL-2) laboratory. The protocols for measuring phosphorus and adjusting pH of cell-free and virus-free cell culture media were optimized at the Ecosystem Ecology Laboratory at the Department of Biology at University of Florida campus in Gainesville, FL.

Cells and Virus Stocks

Vero cells (ATCC, passage 191) derived from the kidney of *Chlorocebus sabaeus* (African green monkey), an adherent cell line that forms a monolayer and is permissive to infection with WNV, were maintained at 35^{o}C in a water-jacketed incubator using Leibovitz's 15 medium (1X) (Gibco™ Gaithersburg, MD). Leibovitz's 15 (L-15) does not require supplementation with CO_2. Vero cells grown without CO_2 supplementation usually take 1-2 days longer than cells grown with CO_2 supplementation to reach confluency (G. Blohm unpublished data). Established procedures for working with Vero cells were adjusted accordingly throughout the experiments.

Virus stocks for these experiments were isolated from *Culex pipiens quinquefasciatus* in Indian River County, FL, in 2006 (isolate # 2186 obtained by plaque-purification), which had been stored at -80^{o}C. The titer of the isolate was obtained immediately upon thawing, before the

start of all experiments, and separate aliquots were stored to avoid RNA degradation by freeze-thawing. To obtain titers, plaque assays were conducted following established procedures with the following modifications: agarose overlay was mixed with 2X L-15 media prepared from powdered L-15; infection was allowed to progress for 1 week, as countable plaques were observed 5-7 days post-infection (as opposed to 2-3 days post-infection normally observed in CO_2-supplemented experiments). Titer of the laboratory stock was consistent with previously recorded titer of the same stock: the working laboratory stock of WNV contained 10^7 plaque-forming units per mL, suggesting that degradation of viral RNA had not occurred since storage.

In the absence of CO_2 supplementation, the laboratory stocks of WNV produced cytopathic effects (CPE) between 5 and 8 days post-infection. The onset of CPE (cell rounding, lysis, cell membrane shrinking and detachment from monolayer) occurred 1-2 days later than recorded in previous studies with CO_2 supplementation. Otherwise all characteristics of the virus are similar to those described in previous studies conducted in a CO_2 supplemented environment (S. Richards and G. Blohm unpublished data).

Phosphorus Manipulations

Cells and virus were exposed to changes in phosphorus by adjusting the concentration of total phosphorus salts in L-15 medium, which contains two forms of phosphorus salts: 0.06 g/L anhydrous monobasic potassium phosphate and 0.19 g/L anhydrous dibasic sodium phosphate (Appendix A: Table 1). We adjusted the concentration of sodium phosphate for our experiments. Because osmotic potential and pH are affected when changing the concentration of salts in cell culture media, we adjusted the pH of the cell culture media with cell culture grade liquid sodium bicarbonate (Gibco™ Gaithersburg, MD) and with HCl. This ensured that at all three phosphorus levels, any changes in cell metabolism and virus attachment rates could be attributed to changes in sodium phosphate ($NaPO_4$) only.

Removal of phosphorus from the cell culture medium requires chelation of phosphate salts, causing the formation of precipitates that are cytotoxic. To prevent the formation of cytotoxic precipitates, we requested custom-made L-15 medium (Gibco™ Gaithersburg, MD) without the addition of sodium phosphate. We then adjusted the concentration of phosphate by addition, rather than removal, of phosphate salts. To achieve phosphorus levels that are close to those of commercially available L-15 media, we added 0.06 g to each L of custom-made L-15 and adjusted pH accordingly. The highest concentration of phosphorus that we could reach without irreversibly changing the pH of the media was at approximately 0.19 g/L of anhydrous dibasic sodium phosphate. At this high concentration of phosphorus, we observed a decrease in pH (from 7.6 to 5.5) that required the addition of 5 – 10 mL sodium bicarbonate. Once the pH reached desired levels, we filter-sterilized the media using a 0.22µM sterile polyethersulfone membrane filter (Millipore® Billerica, MA) and verified total phosphorus concentration by persulfate digestion as described below.

To measure total phosphorus in the cell culture media, we followed a modified version of the persulfate digestion protocol that is commonly used for quantification of total (organic and inorganic) phosphorus during wastewater monitoring surveys. Briefly, 1:10 triplicate serial dilutions of $NaPO_4$ were prepared with custom-made L-15 media (for negative controls, distilled water was used as a matrix), ranging from 0.001 g/L to 1.0 g/L in a clear 96-well plate compatible with microplate reader. Sulfuric acid (11 N) and ammonium molybdate-antimony potassium tartrate (8 g/L) were added to the samples, which are then sealed to block the entrance of CO_2 and incubated for 30 min in the dark. Absorbance readings were then taken for determination of detection limits and standard curve for total mg P/L.

After verification of phosphorus treatment levels and pH adjustment, cell culture medium was then supplemented with 10% heat-inactivated fetal bovine serum (FBS) (Gibco™ Gaithersburg, MD), 1% of 200 mM L-Glutamine (Gibco™ Gaithersburg, MD), 5% of Amphotericin (Fungizone Gibco™ Gaithersburg, MD) and 1% Penicillin Streptomycin Neomycin mix (Gibco™ Gaithersburg, MD) after bringing into the BSL-3 laboratory at FMEL.

Effects of Phosphorus on Rate of Cell Division

We estimated the effect of phosphorus on the population-level growth rate of Vero cells Because we were interested in obtaining an estimate of the effect size of phosphorus on cell population size, as well as the shape of the trajectory of the cell population under different phosphorus environments, we conducted two experiments (end-point and time series).

In the end-point experiment, we seeded eighteen T-25 flasks (six replicates for per phosphorus level) at 10^4 cells per mL. Six days after seeding the flasks, we suspended the cells using trypsin EDTA (Gibco™ Gaithersburg, MD) and counted the number of cells per mL: two 100µL samples of the cell homogenate were obtained for estimation of the cell population size. Live cells were counted using a hemacytometer and 0.4% trypan blue solution (Gibco™ Gaithersburg, MD), a cell-impermeable vital stain which is taken up only by cells that are not viable, thus allowing the distinction between live and dead cells.

In the time-series experiment, we seeded twenty-four T-25 flasks with 10^4 Vero cells per mL (8 flasks for each of the three phosphorus levels) and destructively sampled the cells using trypsin EDTA at four time points for each level of phosphorus: 24, 48, 96, and 168 hours (7 days) post-seeding. Cell counts were conducted as indicated above using trypan blue.

Effects of Phosphorus on Rate of Virus Replication

To determine the effects of phosphorus on the rate of replication of WNV, we conducted two experiments (time-series and end-point). In the time-series experiment we measured the

growth trajectory of the virus through time by real-time RT-PCR at three phosphorus levels. In the second experiment, we quantified the virus by plaque assay at two levels of phosphorus (Low and High) after a 72-hour growth period. To control for indirect effects via changes in the rate of cell division, we varied the seeding density of the cells and allowed them to become 90% confluent before infecting with WNV in both experiments. Cells in the Low P treatment were seeded at 10^5 cells per mL, while cells in the Medium P treatment were seeded at 5 x 10^4 cells per mL and cells at the High P treatment were seeded at 10^4 cells per mL. This allowed all wells to reach confluency at approximately the same time. The wells were inoculated with WNV at an MOI (multiplicity of infection) of 1. The supernatant was then sampled at 8 hour intervals for 72 hours and the virus population was quantified by real-time RT-PCR. In the end-point experiment, we seeded six-well plates at $5x10^4$ Vero cells per mL for the Medium P concentration and at $1x10^4$ virus particles per mL for the High P concentration, at 10 replicates per treatment (20 wells + 4 negative controls that were not infected with virus). When the cells were confluent, we infected each well with 200µL virus stock. After a two hour incubation, we removed the inoculum and refreshed the cell culture media at corresponding P levels. On the 7^{th} day post infection, we sampled the supernatant and quantified the number of virus particles by plaque assay (methods described above).

Results

Adjusting the concentration of phosphorus in the cell culture media led to changes in pH. When compensating for the changes in pH, we were able to isolate the effects of phosphorus alone on the cells and virus populations in cell culture. Cells responded to an increase in phosphorus levels; however the number of virus particles in cell culture did not.

Phosphorus Manipulations

Concentration of total phosphorus in cell culture media varied within 25% of the average for each treatment. At higher levels of phosphorus, the variance in concentration was greater than at lower levels (Figure 3-1)

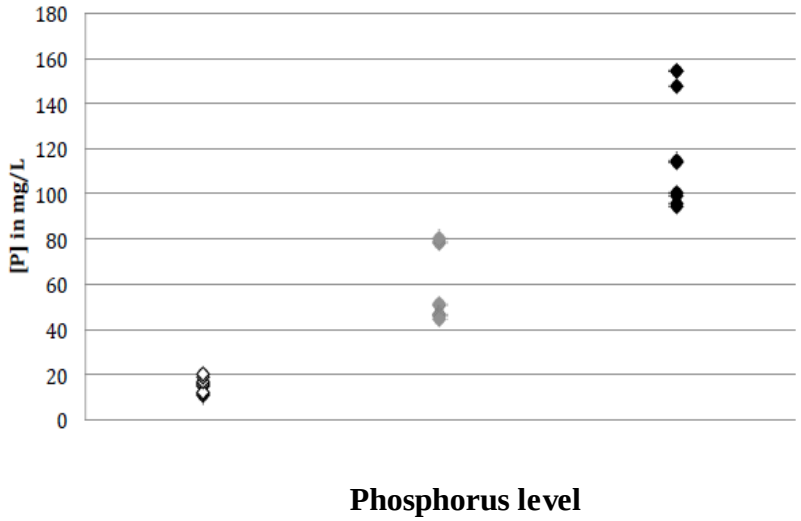

Figure 3-1. Effectiveness of phosphorus treatments. The concentration of total (inorganic and organic) phosphorus for each treatment level. The average concentration of phosphorus in the Low (open diamonds) treatment was 15.1 mg/L; Medium (gray diamonds) was 58.2 mg/L and High (black diamonds) was 119.5 mg/L.

Effects of Phosphorus on Rate of Cell Division

The average rate of cell division increased nonlinearly with an increase in the concentration of phosphorus. A two-fold increase in the concentration of phosphorus led to a 50-65% increase in cell population size after 6 days (Figures 3-2 and 3-3). Effects of phosphorus on cell population size were more variable at higher levels of phosphorus. Due to a low sample size, the shape of the growth trajectory of the cell population at each phosphorus level cannot be determined (Figure 3-3); however the results of both experiments are consistent in that an

increase in the concentration of total phosphorus in the cell culture media leads to an increase in the rate of cell division during a six-day period.

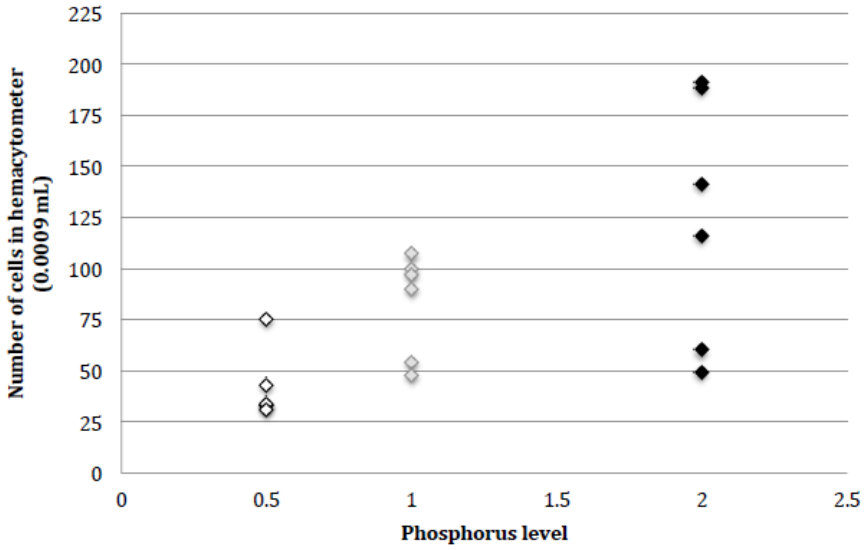

Figure 3-2. Vero cell population size at three phosphorus levels, six days after inoculation. Cells in Low P (open diamonds) conditions reached an average of 41 (± 3 std. error) cells per 0.0009 mL ($4.6x10^4$ cells/mL). Cells in Medium P (gray diamonds) conditions reached an average of 83 (± 4 std. error) cells per 0.0009 mL ($9.2x10^4$ cells/mL). Cells in High P (black diamonds) conditions reached an average of 124 (± 10 std. error) cells per 0.0009 mL ($1.1x10^5$ cells/mL).

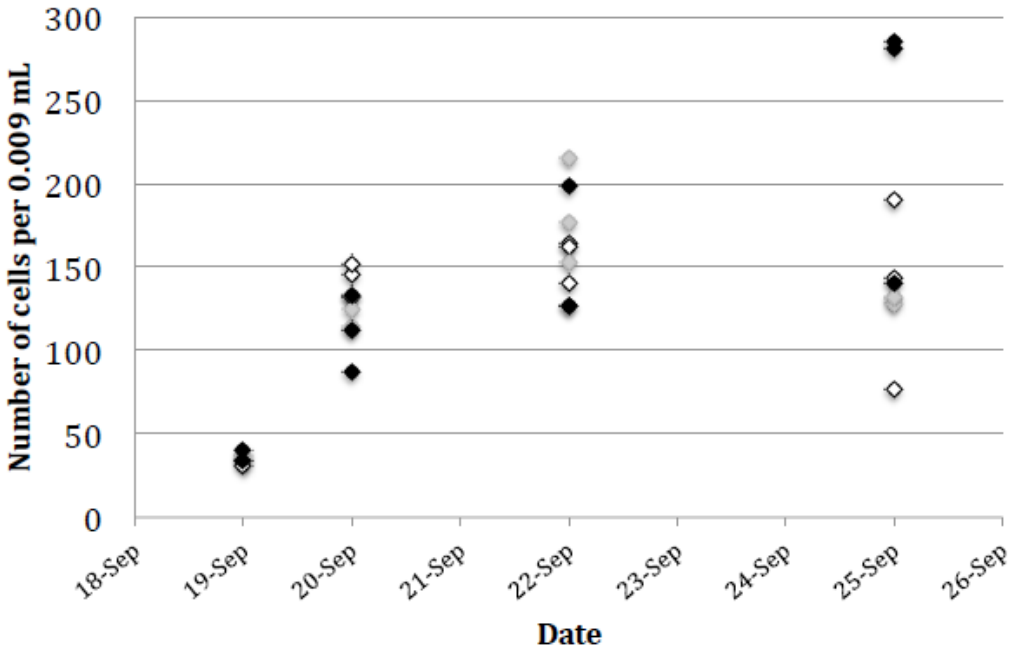

Figure 3-3. Effects of phosphorus on the growth trajectory of Vero cells. During the first three days after seeding, the number of cells in Low P, Medium P and High P is close to 0. In fact, the number of cells in the Low P treatment is slightly higher (147 cells/0.0009 mL) than in the High P treatment (112 cells/0.0009 mL). After six days, the average number of cells in the Low P treatment did not change; however the variance increased. The average number of cells in the High P treatment increased to 208 cells/0.0009 mL).

Effects of Phosphorus on Rate of Virus Replication

There was no effect of phosphorus on the growth trajectory of the WNV population in cell culture (Figures 3-4 and 3-5). Results by real-time RT-PCR show that the virus population in the spent media remains constant for the first 20 hours. The exponential phase of the growth curve occurs at approximately 40 hours post-infection, when the virus population increases from approximately 10^4 virus particles per mL to an average of 10^6 virus particles per mL. The virus population then stabilizes at approximately 75 hours post-infection, when cell lysis begins to

occur (G. Blohm, personal observation) and the virus is unable to continue replicating due to a depletion in the population of available host cells.

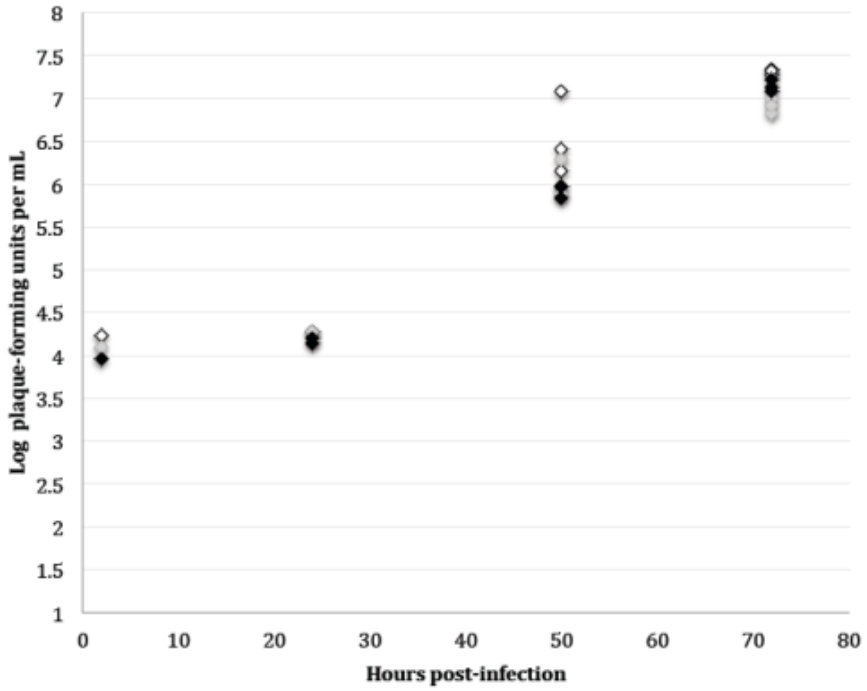

Figure 3-4. Effect of phosphorus on West Nile Virus population size in Vero cells. Number of plaque forming units per mL (determined by q-RT-PCR) of WNV isolate #2186. Low phosphorus is represented by the open circles; medium phosphorus is represented by gray circles, and high phosphorus is represented by black circles. The virus population was grown on confluent monolayers of Vero cells in 6-well plates.

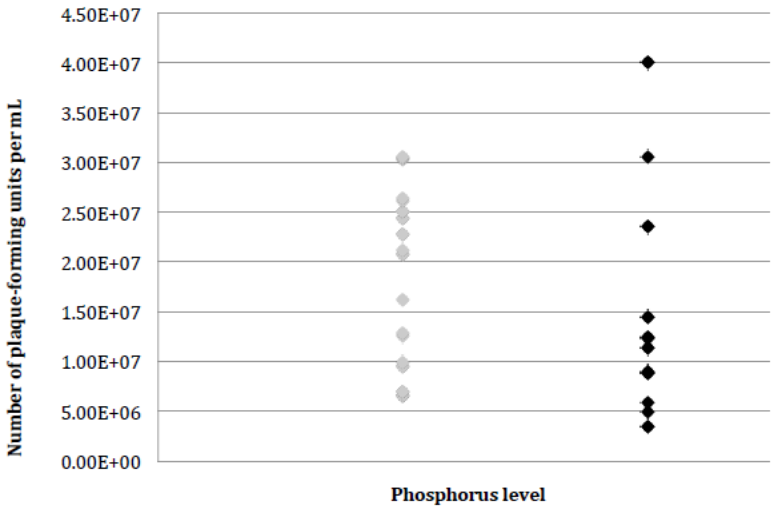

Figure 3-5. Effect of phosphorus on the number of plaque-forming virus particles. Virus populations grown in the Medium P (gray diamonds) treatment reached similar numbers to those grown in the High P (black diamonds) treatment. There was no effect of phosphorus on the final population size of the virus after 7 days of incubation.

CHAPTER 4
MODELING THE REPLICATION OF FLAVIVIRUSES

Flaviviruses (*Flaviviridae*) are single-stranded RNA viruses that are approximately 12 kb in length, containing a capsid protein and a lipid envelope. At the cellular level, attachment and entry proceed by receptor-mediated endocytosis (primarily clathrin-mediated attachment), followed by uncoating in the cytoplasm, where replication and assembly take place. The virus particles then mature in the endoplasmic reticulum and are released as either infectious or defective virus particles. Direct measurement of each step in the virus replication process is often cost-prohibitive. In cases where specific aspects of virus replication cannot be directly measured in the laboratory, it is useful to work with mathematical models and statistical tools for parameter estimation. In a study of *Hepatitis C virus* (HCV), Kumberger et al. (2016) model the within-host dynamics of HCV using a system of differential equations where the cells are distinguished according to their infection status (Uninfected, Infected, and Infectious), with viral entry, viral replication and viral export as rate parameters connecting the three state variables of the host cells. The model is used to predict cell-to-cell transmission in different types of tissue within a host. This approach proved effective at predicting the within-host spread of HCV that had been measured in the literature: in studies where viral maturation was measured by electron microscopy, and where clinical measurements of within-host dissemination of the virus were taken. In Padmanabhan et al. (2011), the molecular process of viral entry was the focus of the model. The authors model the kinetics of virus entry into host cells by including CD81 expression as a determinant of viral entry. Cells resistant to infection due to reduced CD81 expression were included in the model, and as in the previous study, the mathematical model was able to predict results obtained in the literature.

In the section that follows, we model the replication cycle of WNV following an approach that is similar to that of Kumberger 2016, with a few differences detailed below. We focus specifically on the virus population and assume a single state for the cells. We model the growth trajectory of a population of WNV particles in cell culture as a continuous process wherein virus particles attach to the cell, replicate and mature inside the cell, and then are released into the supernatant as infectious virus particles. The rationale for this approach was to divide the replication cycle of the virus into distinct categories that could be measured in the laboratory, thus providing a model that can be tested and improved with published data on WNV replication dynamics and within-host proliferation.

Methods

Model of WNV Replication

We divide the virus population into three sub-populations (V, A, and R) according to their location and infectivity (Figure 4-1). Upon contact with the host cell, infectious virus particles V_t bind to membrane receptors at time t and become incorporated via endocytosis at a rate α. The low pH of the endosome causes the virion envelope to fuse with the endosomal membrane, causing the nucleocapsid to become uncoated at a rate of σ virus particles per unit time. The viral RNA is then released into the cytoplasm, where RNA replication takes place at a rate f. Virion assembly and maturation occur in the endoplasmic reticulum at a rate of β. This rate of assembly and maturation is weighted inversely by the concentration of attached virus particles: $\frac{1}{1+A(t)}$.

It is well-known that WNV replication and maturation are error-prone processes, thus to account for the production of defective (non-infectious) virus particles, we include μ in the equation for R_t to denote the loss of virus particles from the system. Infectious virus particles

enter the supernatant at a rate β and then either become attached to a cell at a rate α or are degraded by RNases and other environmental factors at a rate δ. Figure 4-1 illustrates the trajectory of the virus population in each of the categories.

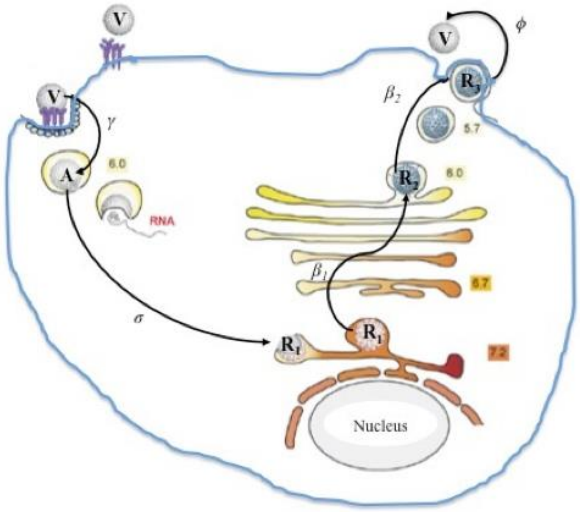

Figure 4-1. Illustration of a generalized *Flavivirus* replication cycle. Virus particles (**V**) become attached (**A**) to the cell membrane. Virus RNA is then released into the cytoplasm, where virus replication occurs. Newly assembled, immature virions enter the endoplasmic reticulum (**R**) and progress along a pH gradient until becoming released back into the extracellular matrix as infectious virus particles.

Mathematical Description of the Model

The model consists of a system of differential equations, each with a positive term and one or more negative terms (Figure 4-2). The positive terms represent the rate of entry of virus particles into a given stage (A, R or V) while the negative terms denote either losses of virus particles from the system or transitions of virus particles from one stage to the next. We chose a continuous time model because WNV establishes a persistent infection, meaning that a cell can be infected multiple times, producing several overlapping generations of virus particles before cell death.

$$\begin{cases} \dfrac{dA(t)}{dt} &= \alpha V(t) - \sigma A(t), \\ \dfrac{dR(t)}{dt} &= \phi\sigma A(t) - \left(\dfrac{\beta}{1+A} + \mu\right) R(t), \\ \dfrac{dV(t)}{dt} &= \dfrac{\beta}{1+A} R(t) - (\alpha + \delta) V(t). \end{cases} \tag{4-1}$$

Stability Analysis for the Endemic Equilibrium

Our WNV model is a system of differential equations that expresses the rate of change of the number of infectious virus particles per mL $V(t)$, the number of virus particles inside the cell $R(t)$ as well as the number $A(t)$ of attached virus particles (Figure 4-1). Setting the equations in the system equal to 0 and solving for the values of A, R, V amounts to finding the values of the state variables for which their rate of change is 0. These are termed the equilibrium values of the state variables. The trivial equilibrium for the model is $A = 0, R = 0, V = 0$. If however, all these equilibrium abundances are positive, such equilibrium is called an "endemic equilibrium". In our case, the non-trivial equilibria are in Equation 4-2

$$V^* = \frac{\phi\beta\alpha - (\beta + \mu)(\alpha + \delta)}{\dfrac{\alpha}{\sigma}\mu(\alpha + \delta)}; \quad A^* = \frac{\alpha}{\sigma} V^*; \quad R^* = \frac{\phi\sigma A^*(1 + A^*)}{\beta + \mu(1 + A^*)}. \tag{4-2}$$

Provided that the numerator of V* is positive, then a simple inspection of all these equilibrium abundances show that these will all be positive. In other words, provided $\dfrac{\phi\beta\alpha}{(\beta + \mu)(\alpha + \delta)} > 1$, these equilibrium abundances will correspond to an endemic equilibrium.

In these differential equation models, the equilibrium values can correspond to concentrations to which the system arrives some time after starting the experiment and subsequently stays there indefinitely, or they can correspond to concentration values that the system quickly gets away

from, if one were to start close to these. In the first scenario, the model is said to have a "stable equilibrium". In the second scenario, where the trajectories of the state variables depart from the equilibrium values, the model is said to admit an "unstable equilibrium". The aim of our stability analysis is to determine when the values of A^*, R^* and V^* above correspond to a stable equilibrium. Below, we show that the same condition, $\frac{\phi\beta\alpha}{(\beta+\mu)(\alpha+\delta)} > 1$, must be met for the endemic equilibrium above to be stable. This stability condition is important because it delineates when a positive amount of free virus particles will persist in the system. In other words, this inequality represents an explicit condition that, if met, will guarantee the long-term persistence of free virus particles in the system (as well as attached and intracellular). Hence, the reproductive number in the system is in Equation 4-3.

$$R_0 = \frac{\phi\beta\alpha}{(\beta+\mu)(\alpha+\delta)} \qquad (4\text{-}3)$$

Assuming that the system is started close to the equilibrium values, the goal of the stability analysis is to study the long-term behavior of the deviations of the system state from these equilibrium values. If the deviations grow indefinitely over time, the equilibrium is unstable. If however the deviations of the system state from the equilibrium values decay towards 0 over time, then the equilibrium is stable, *i.e.*, the trajectories of the state variables A, R, V will eventually converge to their equilibrium values. The system of equations (4-4) follows

$$\begin{cases} \dfrac{dx_1(t)}{dt} = \dfrac{A(t)-A^\star}{dt} = F_1(A,R,V), \\ \dfrac{dx_2(t)}{dt} = \dfrac{R(t)-R^\star}{dt} = F_2(A,R,V), \\ \dfrac{dx_3(t)}{dt} = \dfrac{V(t)-V^\star}{dt} = F_3(A,R,V). \end{cases} \tag{4-4}$$

To study the behavior of the deviations from equilibrium over time, we approximate $\dfrac{dx_i(t)}{dt}$ $(i=1,2,3)$ using a Taylor series expansion around $A^\star, R^\star, V^\star$. Using vector notation by setting $\mathbf{x} = (x_1(t), x_2(t), x_3(t))$, the Taylor series approximation yields the following system of equations, written in matrix format in Equation 4-5:

$$\frac{d\mathbf{x}}{dt} = \mathbf{J}\mathbf{x} = \begin{pmatrix} \dfrac{\partial F_1}{\partial A} & \dfrac{\partial F_1}{\partial R} & \dfrac{\partial F_1}{\partial V} \\ \dfrac{\partial F_2}{\partial A} & \dfrac{\partial F_2}{\partial R} & \dfrac{\partial F_2}{\partial V} \\ \dfrac{\partial F_3}{\partial A} & \dfrac{\partial F_3}{\partial R} & \dfrac{\partial F_3}{\partial V} \end{pmatrix} \begin{pmatrix} x_1(t) \\ x_2(t) \\ x_3(t) \end{pmatrix}. \tag{4-5}$$

Computing these partial derivatives gives the system of equations in 4-6

$$\mathbf{J} = \begin{pmatrix} \sigma & 0 & \alpha \\ \dfrac{R^\star}{(1_A^\star)^2} + \sigma\phi & -\left(\dfrac{\beta}{1+A^\star} + \mu\right) & 0 \\ -\dfrac{R^\star\beta}{(1+A^\star)^2} & \dfrac{\beta}{1+A^\star} & -(\alpha+\delta) \end{pmatrix}. \tag{4-6}$$

As it turns out (Kot 2000), the sign of the eigenvalues λ_1, λ_2 and λ_3 of the Jacobian matrix $\mathbf{J}$ evaluated at the equilibrium determine the trajectories of those deviations because the solution trajectory for the deviations, written in vector format is of the form shown in Equation 4-7

$$\mathbf{x}(t) = \mathbf{c}_1 e^{\lambda_1 t} + \mathbf{c}_2 e^{\lambda_2 t} + \mathbf{c}_3 e^{\lambda_3 t}, \tag{4-7}$$

where the vectors $\mathbf{c}_i$ are constants depending on the model parameters. When all the eigenvalues are negative, as $t \to \infty$, all the terms $e^{\lambda_i t}$ converge to 0, and hence, all the elements in the vector of the deviations of equilibrium $\mathbf{x}(t)$ converge to 0. In other words, as time grows large, if all the eigenvalues of the Jacobian matrix are negative, then the system trajectories converge to the equilibrium values and the equilibrium is said to be stable. Knowing whether the three eigenvalues are negative amounts to verifying that the Routh-Hurwitz criterion (Kot, 2000) holds. For our three-dimensional model system, these criteria are stated in Equation 4-8:

$$\Delta = \left| \mathbf{J} - \mathrm{diag}\begin{pmatrix} \lambda \\ \lambda \\ \lambda \end{pmatrix} \right| = \left| \begin{pmatrix} \sigma - \lambda & 0 & \alpha \\ \dfrac{R^*}{(1_A^*)^2} + \sigma\phi & -\left(\dfrac{\beta}{1+A^*} + \mu\right) - \lambda & 0 \\ -\dfrac{R^*\beta}{(1+A^*)^2} & \dfrac{\beta}{1+A^*} & -(\alpha+\delta) - \lambda \end{pmatrix} \right|. \tag{4-8}$$

This determinant is readily found to be in Equation 4-9

$$\Delta = -(\sigma+\lambda)\left(\frac{\beta}{1+A^*} + \mu + \lambda\right) + \alpha\frac{R^*\beta}{(1+A^*)^2}\frac{\beta}{(1+A^*)} - \alpha\left(\frac{\beta}{1+A^*} + \mu + \lambda\right)\frac{R^*\beta}{(1+A^*)^2} \tag{4-9}$$

Collecting the terms in / in this expression gives a polynomial of degree three of the form $\mathscr{A}\lambda^3 + \mathscr{B}\lambda^2 + \mathscr{C}\lambda + \mathscr{D}$. Straightforward algebraic manipulations of the above expression give $\mathscr{A} = -1$, $\mathscr{B} = \dfrac{-1}{1+A^*}\left(\alpha(1+A^*) + \beta + (1+A^*)(\delta+\mu+\sigma)\right)$,

$$\mathscr{C} = \frac{-1}{(1+A^*)^2}\begin{pmatrix}\alpha((\mu+\sigma)(1+A^*)^2+\beta(1+A^*+R^*))+\\(1+A^*)(\beta(\delta+\sigma)+(1+A^*)(\delta\mu+\sigma(\delta+\mu)))\end{pmatrix}, \text{ and}$$

$$\mathscr{D} = \frac{-1}{(1+A^*)^2}\left(R^*\alpha\beta\mu+(1+A^*)\sigma((\alpha+\delta)(\beta+\mu+A^*\mu)-\alpha\phi\beta)\right).$$

The three solutions to the characteristic equation (Equation 4-10) are the three eigenvalues of $\mathbf{J}$.

$$\Delta = \mathscr{A}\lambda^3+\mathscr{B}\lambda^2+\mathscr{C}\lambda+\mathscr{D} = 0 \qquad (4\text{-}10)$$

The Routh-Hurwitz criterion states that these eigenvalues are all negative (i.e., the equilibrium is stable) provided $\mathscr{B}\mathscr{C}-\mathscr{D} > 0$. Because all the model parameters are positive (otherwise they don't have a biological interpretation), it immediately follows that both $\mathscr{B}$ and $\mathscr{C}$ are negative, and hence their product is positive. Now, determining the sign of $\mathscr{D}$ is more challenging because in the expression above, in the numerator there is a negative sign. However, a part of this numerator is immediately recognized as the negative of the numerator of V^*. Substituting in the expression for $\mathscr{D}$ the explicit values values of R^* and A^*, simplifying and expressing its equation in terms of R_0 gives Equation 4-11

$$\mathscr{D} = (\alpha+\delta)^2\mu\sigma(\beta+\mu)(1-R_0), \qquad (4\text{-}11)$$

Equation 4-11 is negative because all the parameters are biologically valid in our model only when they are positive, and provided $R_0 > 1$. Then, having established that $\mathscr{B}\mathscr{C} > 0$ and that $\mathscr{D} < 0$ if $R_0 > 1$ it follows that the Routh-Hurwitz criterion $\mathscr{B}\mathscr{C}-\mathscr{D} > 0$ holds provided

$R_0 > 1$. Hence, the endemic (positive) equilibrium A^*, R^*, V^* is asymptotically stable whenever the basic reproductive number R_0 is greater than 1, and our proof is complete.

Simulations

We estimated a 'true' value of each parameter and conducted simulations to determine the level of confidence in each parameter when varying sampling frequency. At the start of the experiment, the number of attached virus particles $\mathbf{A}_0$ and the number of intracellular virus particles $\mathbf{R}_0$ are both 0. We initiate virus population growth with a multiplicity of infection (MOI) of 3 virus particles per cell; thus $\mathbf{V}_0 = 3$. To set the initial parameter values, we manually assigned a combination of values that would yield biologically feasible trajectories, where $\mathbf{V}_t$ would stabilize to a carrying capacity and $\mathbf{A}_t$ would remain below $\mathbf{V}_t$.

Assessing the Estimability of the Model Parameters

The estimability of the model parameters was assessed in the context of the data generated by the serial passage experiment. Under this experimental setting, a typical data set consists of a number, say *n*, of virus samples collected from the supernatant at regular time intervals (e.g. if samples are collected every 8 hours for a period of 72 hours that gives us 10 samples if time 0 is included). Then, to assess estimability of the model parameters, the idea is to simulate the trajectories of **A**, **R** and **V** as well as regular random samples from those trajectories at intervals matching the experimental conditions. With those simulated samples, one can then estimate the model parameters and later judge, from the statistical properties of the estimates, the quality of the estimation. Furthermore, here we modified the sampling frequency in order to assess how does the quality of the estimate changes as a function of the number of samples taken, during the same total time period an experiment is running. The specific details of the simulations are given below.

The time series of samples with observation error were then used to estimate via least-squares the model parameters. As stated in Ponciano and Capistran 2011, least-squares estimation amounts to specifying a Normal likelihood. These two steps (simulation and estimation) were the basic building blocks of our simulation experiments. The statistical qualities of the estimates under any given experimental setting can be assessed by running these two steps a large number of times (here we used 100 times for all of our simulation settings). Then, the mean and variance of the estimates, relative to the true parameter values gives precise estimates of the bias and variability of the model parameter estimates.

We assessed the quality of the parameter estimates under two different simulation settings. In the first setting (simulated 100 times), we assumed that for a total of $T = 72$ hours, virus particles were sampled every 1.44 hours, to get a total of 50 observations. Although gathering 50 samples of the supernatant in 72 hours represents substantial experimental work, having a large number of samples gave us a benchmark for assessing the estimability of the parameters. Indeed, in time series statistics, the more samples over time are gathered, the better the quality of the estimate of the dynamics and of the model parameters are. The second experiment consisted of simulating a total of 25 observations taken every 2.88 hours during 72 hours. This setting corresponded to a realistic experimental setting. For this experimental setting we also ran 100 simulation and estimation steps. Finally, for each sampling setting (25 and 50 samples), we assessed the quality of the estimates when one of the parameters was assumed to be known (or estimated empirically from a different experiment), for each one of the model parameters. Thus, for each one of the two settings we initially programmed 7 simulation experiments with 100 runs each (for a total of 700 simulation and estimation steps). The

programs were all written in the language R and as it stands, the computer code takes about 24 hours to run per simulated setting.

Results

The parameters that gave biologically feasible trajectories of the model are shown in Figure 4-4, which presents a simple test of estimability of the model parameters, using 50 simulations. To obtain this figure, I conducted 50 simulations of the A,R,V trajectories with 25 where the deterministic trajectories were contaminated each time with different levels of observation error, (up to 20%). For each simulated time series, I estimated the model parameters using only as observations the time series of V contaminated with observation error. The figure shows that all the estimated parameters fall around the true value, which gave us a quick indication that the model parameters were indeed estimable when one has as data only the time series of the free virus particles. Going from 25 to 50 samples in time only improves the quality of the inference by a little bit, but not substantially (results not shown). When estimating all parameters, all appear unbiased. The variance of the parameter estimates, however, varies widely which indicates that the time series of virus particles contains more information for some parameters than others. For example, Figure 4-3 shows that σ has a large variance and is sometimes over-estimated three to fourfold. Because σ is the most difficult parameter to estimate, when this parameter is known, the remaining parameters are estimated with the highest precision and unbiased for all experiments. Assuming that φ is known yields the worst estimates. Fixing β also gives good parameter estimates but β would be difficult to measure empirically. Fixing μ, δ and α individually improves the precision the estimates of σ and more so when α is the parameter that is fixed.

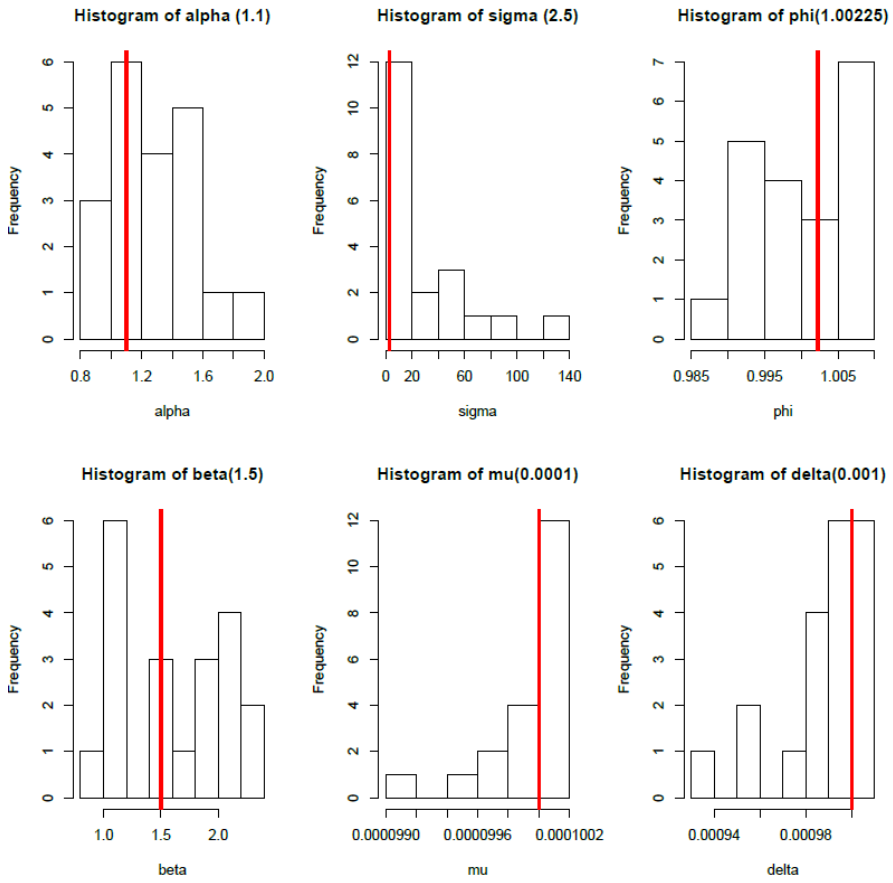

Figure 4-2. Testing the estimability of the parameters. For 50 simulated time series of length 25 all the model parameters were estimated and compared to the true value (horizontal lines in red) used to generate the simulations . In all cases, the parameter estimates fell within the range of values that resulted from the simulations.

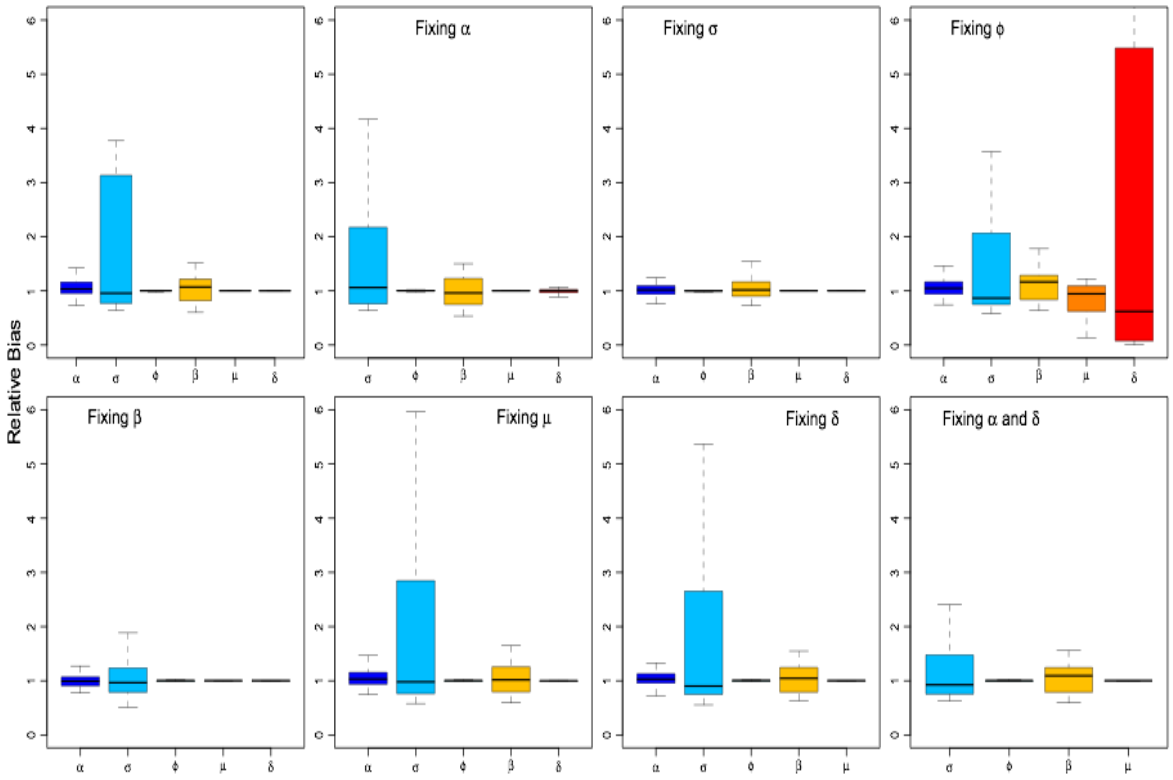

Figure 4-3. Relative bias of each parameter when certain parameters are known, after running 100 simulations for each set of parameters. In the upper left panel, it is assumed that all parameters are unknown. The most difficult parameter to estimate (most uncertain) in this model is β. Fixing (or 'knowing') σ yields the lowest total amount of bias. When φ is fixed, the amount of uncertainty in the model increases.

Discussion

In general, all parameter estimates are unbiased; however the precision varies according to which parameter is known (Figure 4-3). When fixing φ, there is a large reduction in the precision of the model. This parameter appears only once in the system of equations and is multiplied by σ. Thus, fixing it imposes a numerical restriction on the potential optimal solution. These results emphasize that teasing apart the estimates of φ and σ can be challenging. If one could estimate α and δ, one can reduce the variability in the estimates of σ so that now the estimates are on average unbiased and with a precision that frames the estimate within 0.5 and 1.5x relative to the true value (Figure 4-5).

Obtaining values for the parameters in the laboratory poses a different challenge; however the results of the simulations provide guidance on which parameters are most informative, all else being equal. As shown in Chapter 3, V_t can be measured directly as plaque-forming units or, alternatively, by TCID50. To determine the number of defective virus particles that are being produced, the difference between the number of genome copies by real-time RT-PCR and the number of plaque-forming units can be calculated. This will allow an estimation of μ, the rate at which virus particles leave the system either via incomplete maturation or assembly, or due to degradation of viral RNA. Measuring R_t becomes more costly: electron microscopy can be used to visualize the process of virus particle maturation through the endoplasmic reticulum. Direct measurement of A_t and of the kinetics of RNA replication in the cytoplasm (particularly σ) is challenging. By empirically measuring the rate of virus attachment and maturation, it will be possible to obtain statistical estimates of the parameters that cannot be measured in the laboratory.

Estimation of the parameters of a biological, dynamic model using time series data is a common approach in ecological research (Ferguson et al. 2014, 2015a, 2015b). We apply this approach in the field of virology, where we attempt to estimate parameters in the virus replication cycle. We show that when the data at hand consists of time series of observations of one of the stages of the virus replication cycle (V_t), it is possible to estimate with a suitable degree of precision the value of the critical parameters governing the transitions and changes in the virus life-history processes. Although the model is a first and simple representation of the WNV life-cycle, our results represent a substantial step into the formulation of a general understanding of the dynamical processes involved in such life-cycle.

Our simulations and assessment of the statistical properties of the Maximum Likelihood (ML) estimates of the model parameters show how to target efforts aiming at complementing time-series statistical analyses with experimental methods. Because the variance of the parameters varies widely from one parameter to the other, the changes in the observed time series of free virus particles contains more information to estimate some parameters than others. Via our approach where we assumed that one of the parameters at a time was known, we were able to isolate the set of parameters that it would be more valuable to estimate using experimental work. We hope that the results presented here offer guidance and ideas as to which one of these parameters or intra-cellular life-cycle stages it would be most interesting to target in the laboratory.

The model analysis conveys important qualitative predictions. In our analysis, we were able to derive a basic reproductive number for the intra-cellular dynamics of the WNV. This number, being a direct function of the key parameters of the WNV life-cycle, there is much to say and investigate regarding how the persistence of the infectious virus particles can be affected when one or several of these processes is changed. The value of the model then, besides its quantitative prediction is the gain of a qualitative understanding of the conditions under which virus persistence occurs. These predictions could then be scaled up in order to link the intra cellular processes with processes at higher scales involving the vector itself.

CHAPTER 5
CLINICAL CASES: TRANSMISSION OF ZIKA AND OTHER ARBOVIRUSES IN VENEZUELA

Zika virus (ZIKV) continues to spread throughout tropical and subtropical regions of the world. Transmission of ZIKV is known to occur through mosquito bites, from pregnant mother to fetus, through sexual contact, blood transfusion, and accidental laboratory exposure (WHO 2016). It is still unclear whether the virus can be transmitted through saliva, or if post-natal transmission between mother and child can occur during breastfeeding, delivery or close contact between the mother and her newborn. Prior infection with other flaviviruses might affect the severity of ZIKV disease (Dejnirattisai 2016). Little is known about how co-infection with other viruses can affect disease severity and transmission rate.

Our understanding of ZIKV infection is further complicated by the low viremia exhibited in the blood of infected patients. Virus loads are higher in saliva and in urine; furthermore, infected patients appear to shed virus in the urine for months after the acute phase (CDC 2016). Because detection by rt-PCR in patient specimens can sometimes lead to false-negatives when viremia is low, we coupled detection by rt-PCR with virus isolation in cell culture. Results include a case of possible neonatal transmission via breast milk, as well as a possible increase in the incidence of autoimmune complications such as psoriasis (Appendix B).

Methods

In March 2016, a network of doctors was formed and notified of the possible presence of ZIKV in the city of Barquisimeto, Venezuela (pop. 800,000). Participating doctors were briefed on procedures for screening patients for clinical symptoms of possible ZIKV infection (Table X). Informed consent forms and questionnaires were developed and distributed to the network. Specimen collection methods were submitted to the IRB in Barquisimeto and in Florida.

Patients with clinical symptoms of febrile arbovirus infection were sent to the laboratory at Hospital Internacional Barquisimeto. Specimens are being collected following aseptic techniques outlined in hospital protocols and immediately frozen at -150 degrees C in liquid nitrogen. The specimens are shipped by courier to the University of Florida, where they are being tested for ZIKV and other virus infections. Specimens are thawed and handled according to previously established protocols in the Lednicky laboratory at the College of Public Health and Health Professions at the University of Florida, Gainesville. Once screened for ZIKV using primers published by Balm et al. (2012), the specimens will be screened for other Flaviviruses and Alphaviruses using a duplex RT-PCR protocol with genus-specific primers developed by Vieira de Morais Bronzoni et al. (2005). For virus isolation from urine and serum, four cell lines (MRC-5, Vero E6, LLC-MK2 and C6/36) will be inoculated at 60% confluence with aliquots of the specimens. Inoculated cells will be allowed to incubate for 2 hours; checking every 15 minutes for cytotoxic effects of the inoculum. Total inoculation time is adjusted according to cytotoxic effects of the inoculum. Infections will then be allowed to progress for 2-6 weeks depending on the onset of cytopathic effects (CPE). Once CPEs are observed, the spent media will be tested by rt-PCR using the primers mentioned previously.

On March 25, 2016, a 32 year-old female patient from Barquisimeto, Venezuela presented with a 1-day history of symptoms associated with acute ZIKV infection: malaise, arthralgia, conjunctival hyperemia, and maculopapular rash (Figure 4-1). At that time, she was exclusively breastfeeding her 5 month-old child, who was asymptomatic. Breast milk, serum, and urine were collected from the mother on March 28, 2016 (4 days after onset of acute Zika Fever symptoms), and serum and urine from the child the same day, and analyzed as detailed in S1. The mother's urine was positive for ZIKV genomic RNA (vRNA) by real-time RT-PCR (Ct

26.73, level of detection: Ct 36.8). Serologic analyses revealed the mother had IgM and borderline IgG antibodies against ZIKV and no detectable antibodies to Chikungunya virus. She was also IgG positive but IgM negative for Dengue virus (DENV). The mother remained symptomatic with arthralgias and malaise lasting 10 days, with the macular papular rash and conjunctival hyperemia resolving 4 days after the onset of symptoms. The child's serum and urine were positive for ZIKV by real-time RT-PCR, with Ct 35.57 and 35.36. The child remained asymptomatic throughout the observation period. Vero E6 and LLC-MK2 cells were inoculated with aliquots of the mother's milk and urine and child's serum and urine specimens (S1). Cytopathic effects (CPE) characteristic of ZIKV infection were observed 9 and 12 days post-inoculation of the mother's and child's specimens, respectively, onto Vero and LLC-MK2 cells (S2 Figure 2); the breast milk was fractioned, with CPE most obvious in cells inoculated with the lipid-enriched fraction. The presence of ZIKV vRNA was confirmed in all cultures by RT-PCR. Full-genome sequencing of ZIKV isolated from breast milk and the baby's urine (GenBank # KX702400 and KX893855) revealed 99% identity, with only two synonymous nucleotide substitutions at third codon positions between the two strains. Both strains were different from the genomic sequences of other ZIKV strains in the laboratory. Moreover, sequencing of the NS5 gene of the other isolates indicated identical virus was in all specimens from both mother and child; mock-infected cells did not develop CPE, and their spent media was RT-PCR negative for ZIKV vRNA. Phylogenetic analysis showed that the two strains cluster with high bootstrap support (99%) within a larger clade of Colombian sequences (S2 Figure 3). Interestingly, the mother had no history of traveling to Colombia. However, Barquisimeto is on a major trade route to Colombia where a large number of Venezuelans have regularly been traveling recently due to food and medicine shortages in Venezuela. We cannot rule out the

possibility of transmission of an identical viral strain to both mother and infant by a mosquito. However, the mother and child lived in an air conditioned, screened house, where the risk of mosquito transmission would be minimized; they had no recent travel history, and the baby spent most of the time within the house. The finding of live virus in the mother's breast milk is consistent with previous findings (Lednicky et al. 2016); however to date no studies have shown that transmission through breast milk is possible. Matching isolates from her breastfeeding infant is most consistent with post-natal transmission from mother to child. Interestingly, the child, in contrast to the mother, was asymptomatic; assuming that transmission was via breast milk, this provides reassurance that asymptomatic infection can occur in a healthy 5 month old infant infected via breast milk.

Patient Specimens

Blood and urine from mother and child, and breast milk were obtained 28 March, 2016 (4 days after onset of Zika Fever symptoms). Blood (8 mL from mother, 4 mL from baby) were collected into acid citrate dextrose "yellow top" tubes (ACD Vacutainer blood collection tube, Becton Dickinson and Company, Franklin Lakes, NJ). Urine was collected from the mother following a standard mid-stream clean catch method, and by pediatric urine collector bag for the baby. Breast milk was collected into a sterile container after the areola and nipple were cleaned. The specimens were immediately transported to the laboratory at Hospital Internacional Barquisimeto where approximately 1.5 mL of each specimen was aseptically transferred to sterile cryopreservation vials, and all were subsequently stored in the vapor phase of a liquid nitrogen cryotank within 2 hours of collection. A duplicate specimen of the mother's serum was tested for parvo, cytomegalo, Epstein-Barr, varicella zoster and herpes simplex virus types 1 and 2 at Laboratorio Genomik, Maracay, Venezuela following established methods[1]. The remaining

specimens were shipped on dry ice by an express courier to the University of Florida, where the frozen specimens were stored at -80 degrees C upon their receipt on 15 July, 2016.

Cell Culture

Mammalian cell lines LLC-MK2 (CCL-7) and Vero E6 (CRL-1586) were obtained from the American Type Culture Collection (ATCC, Manassas, VA) and propagated as monolayers at 37°C and 5% CO2 in Advanced Dulbecco's Modified Eagle's Medium (DMEM) supplemented with 2 mM L-Alanyl-L-Glutamine (GlutaMAX, Invitrogen,Carlsbad, CA, USA.), antibiotics [PSN; 50 µg/ml penicillin, 50 µg/ml streptomycin, 100 µg/ml neomycin (Invitrogen, Carlsbad, CA, USA)], and 10% (v/v) low IgG, heat-inactivated gamma-irradiated fetal bovine serum [FBS (HyClone, Logan, UT, USA)].

Cell Culture Inoculations

When confluency was at 80%, growth media was removed from cell cultures in T25 cell culture flasks (cell growth surface of 25-cm^2) and replenished with 300 µl of complete media. In preparation for inoculation of the cells, an aliquot of the breast milk was centrifuged to partition lipid-rich and aqueous phases. This was performed to determine whether ZIKV, if present, would survive in a particular fraction of whole breast milk. Separate individual flasks of the cells were inoculated with 200 µL aliquots of the specimens (whole milk, lipid-enriched milk, aqueous-phase milk, plasma, and urine), and incubated at 37°C for 2 hours, with manual rocking of the flasks performed at 15 minute intervals. After 2 hours, 3 ml of additional growth media was added and the cells inoculated at 37°C. Mock-infected cells were maintained in parallel. The cells were observed daily and re-fed with reduced serum media (3% FBS). At the University of Florida laboratory, the cells are maintained and observed for 1 month before being reported as

negative for virus isolation. Spent media from the inoculated cells were sporadically tested by RT-PCR as described previously[2].

Evidence of ZIKV Isolation

Based on the laboratory's cumulative experience with the isolation of ZIKV and as described previously[2], virus-specific cytopathic effects (CPE) consisting of perinuclear vacuoles prior to cell death were expected in ZIKV-infected LLC-MK2 and Vero E6 cells. The ZIKV-specific CPE develop earlier and are more pronounced in LLC-MK2 cells. Cytopathic effects characteristic of ZIKV were observed in all cells inoculated with mother and child's specimens; they were first observed in LLC-MK2 cells 11 days post-inoculation and 1-3 days later in Vero E6 cells. CPE were initially most obvious in LLC-MK2 cells inoculated with lipid-enriched breast milk. No CPE were observed in the mock-infected negative control cells. Representative images of the infected cells are provided in S2.

RT-PCR Screens for Chikungunya, Dengue, and Zika virus RNA

To screen the cultures for *Chikungunya virus* [CHIKV], *Dengue* viruses 1 – 4 [DENV-1,-2,-3, and -4], and ZIKV genomic RNAs, vRNA was extracted from virions in spent cell growth media using a QIAamp Viral RNA Mini Kit (Qiagen Inc., Valencia, CA). The extracted vRNAs were tested by RT-PCR using primers and procedures for CHIKV[3], for DENV types 1–4[4], and for ZIKV[5,6]. Preliminary screens were performed using Omniscript reverse transcriptase (Qiagen) and OneTaq DNA polymerase (New England Biolabs, Ipswich, MA) for PCR.

ZIKV Sequencing

At 14 days post-inoculation, vRNA was extracted from virions in the spent media of LLC-MK2 cells inoculated with mother's milk (lipid-enriched fraction) and child's urine and sequenced as described previously2. Briefly, high-fidelity enzymes [Accuscript High Fidelity

reverse transcriptase in the presence of SUPERase-In RNase inhibitor (Ambion, Austin, TX) and Phusion Polymerase (New England Biolabs)] were used for reverse transcription and PCR. The 5' end was determined using RNA ligase-mediated RACE (RLM-RACE), whereas the 3' was polyadenylated for 3' RACE. Overlapping PCR amplicons were purified and sequenced bidirectionally using Sanger Sequencing using a genome walking strategy and primers described previously2.

ZIKV Phylogenetic Analysis

All currently available ZIKV full genome sequences were downloaded from NCBI (http://www.ncbi.nlm.nih.gov/). Sequences were aligned using ClustalW[7] followed by manual editing with Bioedit[8]. The Maximum Likelihood phylogenetic tree was inferred from the full genome alignment using the best fitting substitution model with the IQTREE program[9], as in our previous study[2]. Statistical robustness and reliability of the branching order within the tree were assessed by bootstrapping (1000 replicates) and fast likelihood-based Shimodaira-Haswgawa (SH)-like probabilities[10] with IQ-TREE.

Serology

Zika virus serologic testing was performed using the Zika Virus ViraStripe® IgG, IgM Test Kit (Viramed® Planegg, Germany). This immunoassay allows the detection of IgG or IgM antibodies against ZIKV specific antigens in human serum. ViraStripe® carries the following purified Zika Virus specific antigens: E, EIII, EIII* (Envelope antigens) and NS1 (Non-Structural antigen 1). The control section of each strip includes a serum control, three conjugate controls and a cut off control. Results of the tests were positive for IgM and borderline for IgG, with low titers suggesting seroconversion.

Results

On March 25, 2016, a 32 year-old female patient from Barquisimeto, Venezuela presented with a 1-day history of symptoms associated with acute ZIKV infection: malaise, arthralgia, conjunctival hyperemia, and maculopapular rash (Figure 4-1).

Figure 5-1. Maculopapular rash on mother's abdomen. Photograph was taken with permission for publication in March 2016.

At that time, she was exclusively breastfeeding her 5 month-old child, who was asymptomatic. Breast milk, serum, and urine were collected from the mother on March 28, 2016 (4 days after onset of acute Zika Fever symptoms), and serum and urine from the child the same day. Blood and urine from mother and child, and breast milk were obtained 28 March, 2016 (4 days after onset of Zika Fever symptoms). A duplicate specimen of the mother's serum was tested for parvo, cytomegalo, Epstein-Barr, varicella zoster and herpes simplex virus types 1 and 2 at Laboratorio Genomik, Maracay, Venezuela. Mammalian cell lines LLC-MK2 (CCL-7) and Vero E6 (CRL-1586) were propagated as monolayers. In preparation for inoculation of the cells, an aliquot of the breast milk was centrifuged to partition lipid-rich and aqueous phases. This was

performed to determine whether ZIKV, if present, would survive in a particular fraction of whole breast milk. After 2 hours, 3 ml of additional growth media was added and the cells inoculated at 37°C. Mock-infected cells were maintained in parallel. The cells were observed daily and re-fed with reduced serum media (3% FBS). Virus-specific cytopathic effects (CPE) consisting of perinuclear vacuoles prior to cell death were expected in ZIKV-infected LLCMK2 and Vero E6 cells. The ZIKV-specific CPE develop earlier and are more pronounced in LLC-MK2 cells. Cytopathic effects characteristic of ZIKV were observed in all cells inoculated with mother and child's specimens; they were first observed in LLC-MK2 cells 11 days post-inoculation and 1-3 days later in Vero E6 cells. CPE were initially most obvious in LLC-MK2 cells inoculated with lipid-enriched breast milk (Figure 5-2). No CPE were observed in the mock-infected negative control cells. Representative images of the infected cells are provided in Figure 5-2.

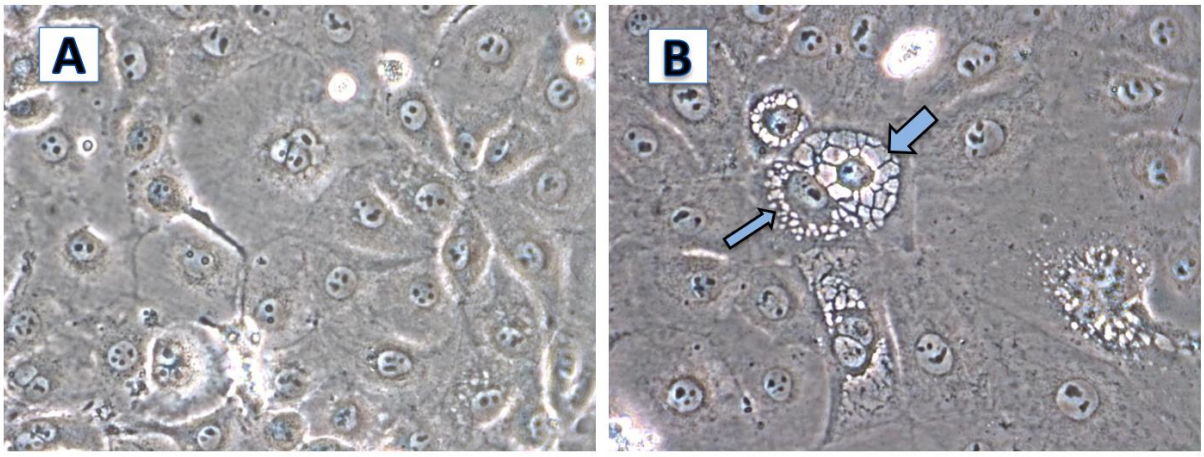

Figure 5-2. Characteristic ZIKV-specific cytopathic effects in LLC-MK2 cells. A. Mock-infected LLC-MK2 cells, 12 days post-seed. Original image magnification at 400X. B. LLC-MK2 cells inoculated with breast milk lipid-enriched fraction, 12 days post-seed. Arrows point out early (small) and late (large) perinuclear vacuoles characteristic of ZIKV infection. Original image magnification at 400X.

At 14 days post-inoculation, vRNA was extracted from virions in the spent media of LLC-MK2 cells inoculated with mother's milk (lipid-enriched fraction) and child's urine and sequenced. Sequences were aligned using ClustalW followed by manual editing with Bioedit.

The Maximum Likelihood phylogenetic tree was inferred from the full genome alignment using the best fitting substitution model with the IQTREE program. Phylogenetic analysis showed that the two strains cluster with high bootstrap support (99%) within a larger clade of Colombian sequences (Figure 5-3).

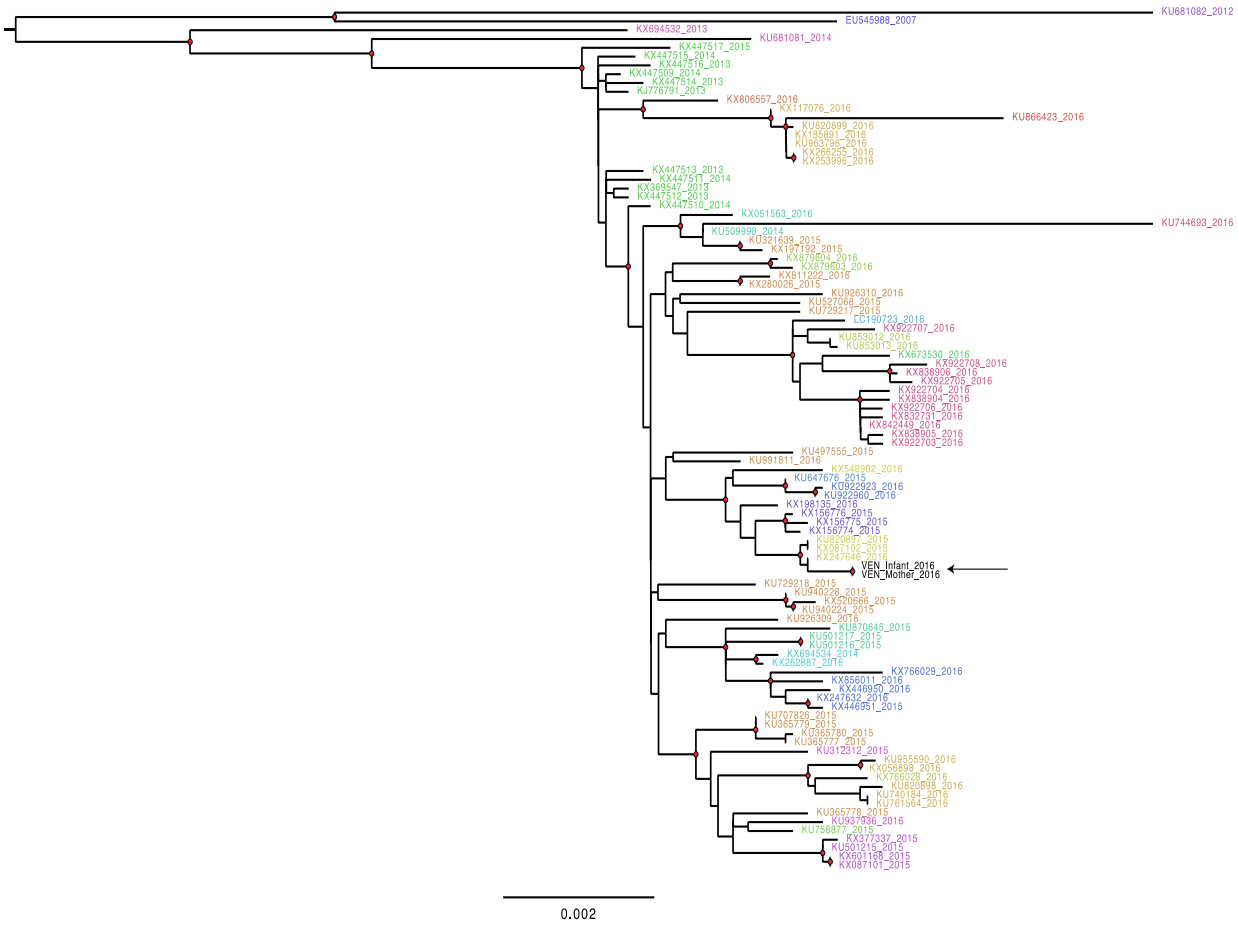

Figure 5-3. Maximum-Likelihood (ML) tree inferred from available ZIKV whole genome sequences. The ML tree was inferred from full genome sequences with the best fitting nucleotide substitution model selected by a hierarchical likelihood test using the program IQ-TREE. All ZIKV full genomes available in GenBank were used. For simplicity only the portion of the tree showing the South American lineage is shown. Sequence labels are colored by country of origin, according to the legend on the left. The sampling year of each sequence is also given in the sequence label. Internal nodes highlighted by red circles have strong bootstrap support (>99%). Arrows indicate the mother and child ZIKV isolates. Branch lengths are scaled in nucleotide substitutions per site according to the bar in the figure.

Discussion

Interestingly, the mother had no history of traveling to Colombia. However, Barquisimeto is on a major trade route to Colombia where a large number of Venezuelans have regularly been traveling recently due to food and medicine shortages in Venezuela. We cannot rule out the

possibility of transmission of an identical viral strain to both mother and infant by a mosquito. However, the mother and child lived in an air conditioned, screened house, where the risk of mosquito transmission would be minimized; they had no recent travel history, and the baby spent most of the time within the house. To date no studies have shown that transmission through breast milk is possible. Matching isolates from her breastfeeding infant is most consistent with post-natal transmission from mother to child. Interestingly, the child, in contrast to the mother, was asymptomatic; assuming that transmission was via breast milk, this provides reassurance that asymptomatic infection can occur in a healthy 5 month old infant infected via breast milk.

CHAPTER 6
CONCLUSIONS AND DISCUSSION

We sought to investigate the role of virulence, transmission mode and environmental context could explain the surge in arboviral disease that has occurred during the past few decades. We combined field data, laboratory experiments, mathematical models and statistical tools to evaluate our findings and to generate predictions across scales of biological organization. Results from the work with *Sigma virus* suggest that mathematical models, when informed by laboratory experiments, can provide a means for extrapolating results to other scales of biological organization, as suggested in Lloyd-Smith 2009 and in Lord 2014. Furthermore, the laboratory-based estimates of virulence were informative enough to accurately predict the field-measured estimates of virus abundance. Interestingly, despite a high frequency of vertical transmission and high virulence, *Sigma virus* persists at high densities in the population of *D. melanogaster* that was sampled. This could be attributed to various aspects of the environmental context such as possible reintroductions of the virus into the *D. melanogaster* population, seasonality of *Sigma virus* abundance, and environmental context such as the fact that our field sites were located along a transect that was adjacent to areas of possibly high fertilizer use.

Given that the populations that were sampled in this study occurred in areas of high agricultural activity, it was sensible to investigate the role of agriculture in determining the prevalence of the virus. To improve our ability to generate predictions concerning arboviruses that are less dependent on strictly vertical transmission, we proceeded to address the next research question by directly studying an arbovirus that exhibits both horizontal and vertical transmission and occurs in areas of high agricultural activity (Reisen 2013). The results from the laboratory experiments with WNV suggest that P could affect virus load indirectly via changes in cell division rates; however we did not detect a direct effect of P on the replication rate of the

virus in cell culture. The absence of this effect could be due to the narrow range of P conditions that were achievable in cell culture. It is also possible that the changes in P that were experimentally induced in the cell culture media were not reflected inside of the cells. Osmoregulatory processes could have maintained homeostatic internal concentrations of phosphorus that did not mirror those in the cell's environment. It's possible that P does not limit virus replication in cell culture. The limiting nutrient could be C, N or another micronutrient. Testing the effects of P on vector competence could yield results that are different from those obtained in cell culture. Effects of P on other aspects of mosquito biology, which could affect vector competence, were quantified experimentally by Peck et al. (2005) in *Cx. pipiens quinquefasciatus* and in *Cx. pipiens tarsalis*, two competent vectors of WNV. An increase in the rate of larval development was observed for one species, where P led to earlier emergence and smaller size at emergence. One issue with this work was that the experimental increase in P led to high mortality, thus sample sizes were low. Future work should include experiments where total P is increased following alternative protocols that cause less mortality to the larvae. Given that larval stoichiometric ratios mirrored those of the environment, it would be interesting to determine whether those stoichiometric signatures are maintained throughout the lifespan of the mosquitos, and the effects of larval nutritional ratios on future reproductive success of females should be investigated, given that gonadal tissue tends to be higher in per-unit-mass concentration of P. Finally, future work should measure other aspects of vector competence such as lifespan. The fact that a positive effect of P was observed at the landscape level and at the individual level in other systems suggests that the results from cell culture could not hold across all scales of biological organization. According to metabolic theory (Sterner 2002), we expect a negative relationship between mass-specific metabolic demands of P and lifespan. Thus, it is

possible that faster-growing mosquitoes could have lower vector competence due to fewer opportunities for bloodfeeding. Because of these results, the original model of virus replication was modified so that P was kept out of the system of equations.

The literature on mathematical models of within-host Flavivirus dynamics is focused primarily on HCV. These models involve systems of differential equations where the replication rate of the virus is modeled as a function of various aspects of cell membrane composition, gene expression, and others. Models of the role of intracellular pH, which is regulated by P, are nonexistent to our knowledge. Our model attempts to incorporate the possible pathways by which P could affect WNV population dynamics within a host. Furthermore, we apply statistical tools developed in ecological population biology (Ferguson et al. 2014, 2015a, 2015b) to determine the accuracy with which we can estimate the rate of virus attachment, replication, maturation and exit from an infected cell. Initial estimates of these parameters all included the expected mean or 'true' parameter value. We were able to estimate the rate of virus attachment, entry, and exit from the cell with relatively higher confidence than other parameters. The most difficult parameter to estimate is the rate of virus replication and assembly within a cell. This is also difficult to measure in the laboratory. Improvements to our model of intracellular replication could draw from HCV studies (Dahari 2007, Padmamabhan 2011); for viral assembly from phage research (Zlotnick 2011) and for maturation and assembly in the endoplasmic reticulum (Romero-Brey 2016).

Results from the study in Venezuela suggest that transmission mode could be a dynamic process that is not only a function of virulence, but a function of immunological history of the host. The role of co-infections should also be investigated, as preliminary evidence suggests that two of the patients infected with ZIKV were also infected with DENV4 (Blohm unpublished

data). Testing clinical specimens for multiple viral infections when patients present with febrile illness is important for understanding the basic virology and epidemiology of arboviruses. Second, prior immunological history of the patient can determine virulence and therefore the evolutionary trajectory of the host and of the virus. As indicated in Appendix B, patients with prior history of autoimmune diseases experienced greater susceptibility and a wider range of complications in response to infection with ZIKV than patients that do not have prior exposure to either ZIKV or a closely related Flavivirus such as DENV4. When an accurate, specific antibody test for DENV and ZIKV is developed, it will be possible to assess the role of prior infection with closely related viruses on clinical outcomes of infection. Continued work that is multidisciplinary in its approach will lead to the development of improved predictive models, tools for clinical diagnosis in resource-limited settings, and a deeper understanding of the factors that give rise to the establishment and persistence of arboviruses. The combination of model system approaches, mathematical models, and laboratory experiments is a fruitful source of information about clinically important arboviruses.

APPENDIX A
FORMULATION OF CELL CULTURE MEDIUM

Table A-1. Formulation of L-15 cell culture medium.

Components	Molecular Weight	Concentration (mg/L)	mM
Amino Acids			
Glycine	75	200	2.6666667
L-Alanine	89	225	2.52809
L-Arginine	174	500	2.8735633
L-Asparagine	132	250	1.8939394
L-Cysteine	121	120	0.9917355
L-Glutamine	146	300	2.0547945
L-Histidine	155	250	1.6129032
L-Isoleucine	131	250	1.908397
L-Leucine	131	125	0.9541985
L-Lysine	146	75	0.51369864
L-Methionine	149	75	0.5033557
L-Phenylalanine	165	125	0.75757575
L-Serine	105	200	1.9047619
L-Threonine	119	300	2.5210085
L-Tryptophan	204	20	0.09803922
L-Tyrosine	181	300	1.6574585
L-Valine	117	100	0.85470086
Vitamins			
Choline chloride	140	1	0.007142857
D-Calcium pantothenate	477	1	0.002096436
Folic Acid	441	1	0.002267574
Niacinamide	122	1	0.008196721
Pyridoxine hydrochloride	206	1	0.004854369
Riboflavin 5'-phosphate Na	478	0.1	2.09E-04
Thiamine monophosphate	442	1	0.002262444
i-Inositol	180	2	0.011111111
Inorganic Salts			
Calcium Chloride (CaCl2) (anhyd.)	111	140	1.2612612
Magnesium Chloride (anhydrous)	95	93.7	0.9863158

Magnesium Sulfate (MgSO4) (anhyd.)	120	97.67	0.8139166
Potassium Chloride (KCl)	75	400	5.3333335
Potassium Phosphate monobasic (KH2PO4)	136	60	0.44117647
Sodium Chloride (NaCl)	58	8000	137.93103
Sodium Phosphate dibasic (Na2HPO4) anhydrous	142	190	1.3380282
Other Components			
D+ Galactose	180	900	5
Phenol Red	376.4	10	0.026567481
Sodium Pyruvate	110	550	5

APPENDIX B
MANUSCRIPTS IN PREPARATION: CUTANEOUS MANIFESTATIONS OF ZIKV

Generalized pustular psoriasis triggered by Zika virus infection.

Alberto E Paniz Mondolfi[1,2], Marier Hernandez Perez[3], Gabriela Blohm[4], Marilianna Marquez[5,6], Adriana Mogollon Mendoza[5,6], Carlos E Hernandez Pereira[5,6], Julia Rothe DeArocha[7], Alfonso J Rodriguez Morales[8].

Affiliations: *[1] Department of Tropical Medicine and Infectious Diseases, Hospital Internacional Barquisimeto, Lara, Barquisimeto, Venezuela. [2]Instituto Venezolano de los Seguros Sociales (IVSS), Department of Health, Caracas, Venezuela; [3]Department of Dermatopathology, Miraca Life Sciences Research Institute/Tufts Medical Center, Boston, MA, USA; [4]Department of Biology, College of Liberal Arts and Sciences, University of Florida, Gainesville, FL, USA; [5]Infectious Diseases Research Incubator and the Zoonosis and Emerging Pathogens regional collaborative network. [6]Health Sciences Department, College of Medicine, Universidad Centroccidental Lisandro Alvarado, Barquisimeto, Lara, Venezuela; [7]Psoriasis Unit, Hospital Central "Antonio Maria Pineda", Barquisimeto, Lara, Venezuela. [8] Public Health and Infection Research Group, Faculty of Health Sciences, Universidad Tecnológica de Pereira, Pereira, Colombia.*

***Keywords*:** *Zika virus*; psoriasis; viral, cutaneous.

Running title: Psoriasis triggered by Zika virus.

Correspondence: Alberto E Paniz Mondolfi MD, MSc, FFTM RCPS (Glasg), Yale-New Haven Hospital, Microbiology Laboratory (PS656), 55 Park Street, New Haven CT 06511 (alberto.paniz-mondolfi@yale.edu, albertopaniz@yahoo.com).

Abstract

Zika virus (ZIKV) is an emerging arthropod-borne virus belonging to the flaviviridae family (1) which is expanding in epidemic proportions through tropical and subtropical areas around the world (1). Its clinical presentation is non-specific being usually misdiagnosed with other classical viral exanthems and arboviral infections such as Chikungunya (CHIKV), Dengue (DENV) and Mayaro (MAYV) (1, 2), thus posing a challenge at the time of diagnosis. The emergence of ZIKV has been linked to the development of a number of clinical complications, mainly congenital and neurological (1). Yet, besides its self-limiting pruritic maculo-papular rash, little is known about the biology and cutaneous manifestations of ZIKV disease.

Infections are amongst the well-known triggers of psoriasis (3). Herein, we report an exceptionally interesting case of psoriasis presenting three weeks after an otherwise uneventful resolution of an acute ZIKV infection.

Report

A 68-year-old woman presented with a 10-day history of generalized erythroderma and scaly plaques of acute onset. She also complained of general malaise, fever and localized tenderness. Three weeks prior, she had developed a pruritic maculo-papular rash along with asthenia, small joint arthralgias and conjuctival hyperemia, which resolved uneventfully after 5 days. At that time a full blood count and chemistry were unremarkable except for mild lymphocyte leukocytosis. Serologic analyses using the Zika Virastripe® IgG/IgM test kit (Viramed®, Planegg, Germany)

revealed a positive IgM and negative IgG. Additional serologic testing for DENV, CHIKV, EBV, CMV and parvovirus returned negative. RT-PCR for DENV and CHIKV were negative but positive for ZIKV.

On physical examination the patient exhibited extensive erythorderma and sharply demarcated erythematous silvery scaly round-to-oval plaques. Most plaques harbored obvious coalescing macroscopic pustules forming large central crusts (Fig. 1 a, b). Lesions started as erythematous macules exhibiting an abrupt centrifugal expansion in a period of hours. Interestingly, most lesions localized to trunk and proximal aspects of limbs (were the original ZIKV-associated rash was more pronounced).

Histological examination revealed psoriasiform epidermal hyperplasia with horizontally confluent parakeratosis and neutrophil exocytosis (Fig. 1a) at the lesion edges along with intraepidermal (subcorneal) neutrophilic pustules towards the center, and a mixed dermal lymphocytic and neutrophil infiltrate.

At admission, the complete blood count, chemistry and hepatic transaminase tests were normal with an elevated C-reactive protein of 98 mg/L (normal < 10 mg/L). Screening for other infectious agents including hepatitis A, B and C, HIV and syphilis was negative. Antistreptolysin O titers returned negative as well. The patient was initiated on intensive topical therapy with class 1 steroids (Clobetasol propionate 0.05% BID) and methotrexate at a starting dose of 7.5 mg weekly. Her symptoms gradually resolved with persistence of a few large lesions that eventually faded after 15 weeks. She did not report any side effects and laboratory values remained normal.

Discussion

Psoriasis is a chronic skin disease that affects approximately 2% of the population (4) with many triggering factors, both external and systemic capable of inducing the disease phenotype in susceptible individuals (4). Compelling evidence suggests that many microorganisms may play a role in the onset or exacerbation of psoriasis (3). Bacterial agents such as streptococci and staphylococcus are considered the most common players implicated in the development of the disease, presumably through superantigen activation of skin-seeking T cells (3).

Other agents linked to the pathogenesis of psoriasis include fungi like *Malassezia* and *Candida sp*. which through colonization may elicit an up-regulation of keratinocyte expression promoting a hyperproliferative state and also producing T cell activating superantigenic factors in a similar fashion to pyogenic bacteria (3). In addition, infection with viral agents such as retroviruses (3), EBV (5), VZV (6), CMV (5), HPV (3) and HSV (7) have also been associated with the onset of psoriasis. Moreover, a recent study has suggested the potential role of CHIKV as a trigger for psoriasis (8).

Although viral triggers have been implicated in the pathogenesis of psoriasis the exact mechanisms driving its progression have not been well established. The exact mechanism driving the pathogenesis of ZIKV at the cutaneous level remains unclear. However recent evidence reveals that human keratinocytes are permissive to ZIKV replication in early stages of infection with notable cytopathic effects and induction of apoptosis (9). This initial interplay between the virus and the keratinocyte sets the scene for the development of the psoriatic plaque initiating events,

including activation and production of type 1 interferons (IFN) via specific induction of pattern recognition receptors (PRRs) and up-regulation of expression of IFN-stimulated genes (OAS2, ISG15 and MX1) as well as chemokines (such as CXCL10, CXCL11 and CCL5) which promote T-cell attraction and direct receptor independent-like antimicrobial activity (9).

In addition, the polyfunctional T cell activation (Th1, Th2, Th9 and Th17 response) seen during the acute phase of ZIKV-infected patients (10) along with recent evidence that suggest that up to 50% of human in-vitro generated immature dendritic cells (DCs) challenged with ZIKV express virus envelope proteins (favoring propagation of the virus in the human skin) (9); further support a role for aberrant activation of dermal DCs´ which would stimulate auto-reactive Th17 cells and cytokines inducing keratinocyte activation and epidermal proliferation.

To the best of our knowledge this is the first report linking ZIKV as a possible trigger for psoriasis. Experimental evidence suggests that the virus directly contributes to the release of keratinocyte-derived mediators of the inflammatory process and the T-cell driven immune reaction that drive the evolution of the psoriatic reaction. The association reported in this case provides important clinical insights for further studies.

References:

1. Musso D, Gubler DJ. 2016. Zika virus. *Clin Microbiol Rev* 2016 Jul;29(3):487-524.
2. Paniz-Mondolfi AE, Rodriguez-Morales AJ, Blohm G et al. ChikDenMaZika Syndrome: the challenge of diagnosing arboviral infections in the midst of concurrent epidemics. *Ann Clin Microbiol Antimicrob* 2016 Jul 22;15(1):42.

3. Fry L, Baker BS. Triggering psoriasis: the role of infections and medications. *Clin Dermatol* 2007 Nov-Dec;25(6):606-15.
4. Nestle FO, Kaplan DH, Barker J. Psoriasis. *N Engl J Med* 2009 Jul 30;361(5):496-509.
5. Jiyad Z, Moriarty B, Creamer D et al. Generalized pustular psoriasis associated with Epstein-Barr virus. *Clin Exp Dermatol* 2015 Mar;40(2):146-8.
6. Ito T, Furukawa F. Psoriasis guttate acuta triggered by varicella zoster virus infection. *Eur J Dermatol* 2000 Apr-May;10(3):226-7.
7. Zampetti A, Gnarra M, Linder D et al. Psoriatic Pseudobalanitis Circinata as a Post-Viral Koebner Phenomenon. *Case Rep Dermatol* 2010 Nov 6;2(3):183-188.
8. Seetharam KA, Sridevi K. Chikungunya infection: a new trigger for psoriasis. *J Dermatol* 2011 Oct;38(10):1033-4.
9. Hamel R, Dejarnac O, Wichit S et al. Biology of Zika Virus Infection in Human Skin Cells. *J Virol* 2015 Sep;89(17):8880-96.
10. Tappe D, Pérez-Girón JV, Zammarchi L et al. Cytokine kinetics of Zika virus-infected patients from acute to reconvalescent phase. *Med Microbiol Immunol* 2016 Jun; 205(3):269-73.

Cutaneous features of Zika virus infection: A clinicopathological overview.

Paniz-Mondolfi AE, Blohm GM, Hernandez-Perez M, Larrazabal A, Moya D, Marquez M, Talamo A, Rothe J, Lednicky J, Morris JG.

1. Introduction:

Zika virus (ZIKV) is an arbovirus belonging to the *Flaviviridae* family, which was first isolated serendipitously in non-human primates (Rhesus monkeys) and mosquitoes in 1947-1948 in the Zika forest of Uganda (X). Its first isolation in humans was in 1954 in Nigeria (X), although many cases were later recorded through almost half a century during yellow fever serological survey studies in Africa. ZIKV has emerged over the past decades causing minor outbreaks around Africa and Asia; however, it wasn't until 2007 that the first major outbreak was reported in the Western Pacific island of Yap (Federated States of Micronesia), followed later by a larger epidemic in French Polynesia through 2013 and 2014 (X). Recently in 2015, ZIKV reached the shores of the Americas following the footsteps of other arboviruses such as Chikungunya (CIHKV) and causing great concerns due to its unprecedented pathogenicity and increased risk for causing severe fetal malformations and neurological symptoms. Even though Zika virus infections are usually mild or remain clinically unapparent (X), cutaneous manifestations as for other arbovirosis remain a hallmark of the disease. In this article, we discuss the cutaneous clinical spectrum of ZIKV infection, while comprehensively revising the main biological aspects of the virus and its interaction with human skin cells, the host immune response and pathogenesis.

2. Etiology and Epidemiology:

ZIKV is a Flavivirus closely related to the Yellow fever virus in the Spondweni (SPOV) clade of X mosquitoe-borne Flaviviruses (X). It is an enveloped virus that is approximately 50 nm in diameter and contains a 10.794 kb single stranded, positive sense RNA genome (X). The genome consists on two flanking no coding regions (5'NCR and 3'NCR) and an open reading frame coding for a polycistronic peptide that yields three structural (capsid [C], premembrane/membrane [PrM], and envelope [E]) and seven nonstructural proteins, NS1, NS2A, NS2B, NS3, NS4A, NS4B, and NS5 (X). Molecular epidemiology studies suggest that the virus emerged in East Africa around 1920 differentiating into two distinct African clusters, and later believed to have migrated to Asia in the 1940s originating the Asian lineage strains (X). To date, phylogenetic studies conducted by Lanciotti et al. after the recent Yap State outbreak confirm the existence of three different ZIKV lineages or subclades: East African (prototype Uganda strain), West African (Senegal strains), and Asian (ZIKV 2007 Yap strain) (X). It is believed that ZIKV reached the Americas through introduction of an Asiatic lineage strain in Brazil as early as in 2013 (X), yet many aspects such as it's increased pathogenicity observed during the New World epidemics remain to be elucidated.

It is an arthropod-borne virus, which is transmitted mainly by *Aedes* species of mosquitoes. It was first isolated from *Aedes africanus* (X) and later in a wide range of other *Aedes* species such as *Ae. apicoargenteus*, *Ae. vittatus*, *Ae. furcifer* and *Ae. luteocephalus*, being the principal vectors of transmission *Aedes aegypti* and *Aedes albopictus*. Other authors have reported the presence of the virus in other species such as *Culex sp* (X), *Mansonia uniformis*, *Anopheles coustani*, and *Culex perfuscus*, nevertheless their role as competent vectors remains to be proven. (X).

In rural settings, reservoirs include non-human primates and many other mammalian species (X); however in urban cycles humans may act as the main hosts (X). Though not much is known about its ecology, ZIKV transmission is thought to occur mainly in sylvatic cycles with consequent spillovers to rural and urban settings influenced by a number of epidemiological factors such as switch in vector usage, the emergence of new strain variants (X) and other geographic and climatic factors influencing biomes and transmission dynamics (X).

Nonvectorial transmission has been reported to occur directly from mother to child (X), by transfusion (X), through saliva (X), sexually (X) and presumably via breastfeeding (X).

3. Pathogenesis:

The exact mechanisms driving the pathogenesis of ZIKV at the cutaneous level remains unclear. Nevertheless a recent study by Hamel et al. has provided important insights into the interaction of ZIKV and human skin cells (X). Similarly to other arboviruses, ZIKV infects the host by vector-mediated transmission through blood-feeding by female mosquitoes (X) who injects the virus into the skin allowing it to infect cutaneous resident cells such as dermal macrophages and skin fibroblasts (X). In these cells, the virus will drive its first replication cycle, thus triggering an initial immune response from the host as observed with other arboviruses (X). The concurrent delivery of several well-known constituent's on the mosquito saliva aid in the potentiation and capacity of arboviruses, such as ZIKV to replicate at the anatomical site of inoculation (X), leading to an increased viremic phase of the disease in the vertebrate host (X) and it´s dissemination to other tissues causing acute viral symptoms (X).

Because skin cells are the first to encounter arboviral pathogens after their inoculation in the host, the identification of susceptible cell types is of pivotal importance on elucidating the main pathogenic aspects of ZIKV infection. Some of the cells have shown to be permissive to the installment of infection via interaction with specific receptors of the mammalian host (X). Studies in human skin cells using a strain isolated from the recent outbreak in French Polynesia have shown that epidermal keratinocytes, immature dendritic cells and dermal fibroblasts are permissive to infection by ZIKV (X). Such permissiveness driving the entry of the flavivirus into the host cell seems to be driven by its interaction with a variety of cell surface receptors and attachment factors such as the sulfated polysaccharide heparan sulfate which is widely known as a non-specific attachment factor for flaviviruses (X). However, over a dozen putative receptors and attachment factors have been described to play a role in the entry of flaviviruses into mammalian and mosquito cells to date. More recently, the dendritic cell-specific intracellular adhesion molecule 3-grabbing non-integrin (DC-SIGN), a type of C-type lectin receptor, was demonstrated to play an important role on mediating ZIKV internalization in immature dendritic cells (X). This is in lines with previous studies where it has been demonstrated that DC-SIGN plays a major role in Dengue virus (DENV) pathogenesis as well (X).

In addition to DC-SIGN, other entry / adhesion factors have shown to participate in ZIKV infection and internalization at the skin level. Such is the case of the AXL tyrosine kinase receptor (AXL), Tyro3 tyrosine kinase receptor (Tyro3) and the TIM-1 protein (X). In human skin, it has been shown that AXL strongly enhances ZIKV infection in synergy with TIM-1, probably with TIM-1 acting as a viral binding factor and later transferring it to AXL in order to initiate internalization (X). However, it is presumed that TIM-1 is not indispensable for ZIKV endocytosis and that it rather may act by concentrating virions in the cell surface in order to

facilitate their interaction with AXL raising the interesting concept of "receptor cooperation" (X).

Another important aspect to consider is the fact that ZIKV can infect and replicate in several of the cell constituents of the cutaneous milieu such as epithelial, mesenchymal, endothelial and immune-cell lineages exhibiting at the same time a selective tropism for certain cells which is determined by the profile of receptor expression (X). In this sense, for example while immature dendritic cells express DC-SIGN, epidermal keratinocytes and cutaneous fibroblasts lack this receptor but in turn express AXL which has proven to play a major role in ZIKV entry (X). Such a wide range of entry receptors provides the virus with an enhanced capacity to infect a variety of target cells in the skin.

Even though the epidermis serves as an important mechanical barrier against physical and environmental aggressions, arboviruses such as ZIKV have managed to subvert this protective blockade by reaching the sensitive cell targets using the arthropods buccal apparatus to penetrate the thickness of this robust outer compartment. But as briefly mentioned above, the epidermis is home to three major resident cell populations (keratinocytes, melanocytes and Langerhans cells), which play an important role in the initial homing and replication of ZIKV and which deserve to be examined in more detail in the following lines.

3.1. Keratinocytes

Keratinocytes constitute the major cell population of the epidermis, playing an essential role in maintaining the infrastructure responsible for maintaining the barrier function through its differentiation into the outmost cornified layer (X). However, it is in the innermost layers of the epidermis were an intricate network of hormones and cytokines orchestrate the interaction of

keratinocytes with other specialized cells to drive key immune and metabolic functions (X). Studies on cellular tropism have revealed that epidermal keratinocytes are the initial target for West Nile virus infection (X) as well as early DENV replication (X). Similarly Hamel et al. have explored the contribution of primary human epidermal keratinocytes obtained from neonatal foreskin in the early stages of ZIKV infection, proving the permissive nature of human keratinocytes in ZIKV replication (X) as well.

In addition, the gradual increase in the production of ZIKV particles in human keratinocytes along with the cytopathic effects observed in experimentally infected cells (X), signal the occurrence of ongoing apoptosis (X). As observed in CHIKV (X), WNV (X) and DENV (X), apoptotic blebs serve as shelter for the virus allowing it to evade the host's cellular and humoral immune response (X). In these same lines, it has been speculated that apoptosis in ZIKV follows this same strategy aiming to escape the immune response from the host by increasing their dissemination to neighboring healthy cells (X).

From an immunological standpoint keratinocytes are known to play a key role in innate immunity via pathogen recognition (X). The type 1 interferon (IFN) pathway is perhaps one of the most important anti-viral pathways, with particular relevance in CHIKV (X) and DENV (X) infections. Activation and production of type 1 IFNs are triggered through pattern recognition receptors (PRRs) following recognition of pathogen-associated molecular patterns (PAMPs) (X). Amongst the most important pattern recognition receptors are the Toll-like receptors as well as the cytosolic retinoic acid-inducible gene 1 (RIG1) like receptors MDA-5 (melanoma differentiation-associated protein 5) and RIG-1 (X). As with DENV (X) and WNV (X) infections, ZIKV strongly induces the expression of important PRRs such as TLR3, MDA-5 and RIG-1 (X). However, type 1 IFN production in ZIKV infection appears to occur in an

independent fashion to IRF3 (X) as observed for other different viruses (X), in both flavivirus-infected epidermal keratinocytes and dermal fibroblasts (X).

3.2. Cutaneous fibroblasts

Cutaneous fibroblasts also remain in the epicenter of ZIKV pathogenesis. Experimental evidence suggests that this cell population constitutes a site for active viral replication (X). As in keratinocytes ZIKV induces an innate anti-viral response with specific induction of PRRs, upregulation of TLR3 mRNA expression, as well as enhanced transcription of RIG-1 and MDA5, thus promoting the initiation of downstream signaling pathways aimed to activate the antiviral machinery (X). In a similar fashion, ZIKV infection is known to upregulate the expression interferon stimulated genes (OAS2, ISG15 and MX1), and chemokines (such as, CXCL10, CXCL11 and CCL5) (X) which promote T cell attraction and direct, receptor-independent defensin-like antimicrobial activity (X). It is in this dermal infection phase, where as in CHIKV infection fibroblasts located in the deep dermis and basal skin layer may become permissively infected, thus allowing viral replication (X) including other skin resident cells like macrophages, endothelial and muscle cells (X).

Interestingly, experimental evidence using electron microscopy to visualize ZIKV-infected skin fibroblasts has shown characteristic autophagosome-like vesicles in these cells (X). Although autophagy is known to occur as a physiological response to cellular stress following virus amplification (X), recent evidence suggests that such process may serve viruses as a survival strategy to further increase their replication supporting their life cycle (X). Virus-induced induction of autophagy, also known as proviral autophagy seems to play a role in replication and translation processes of many arboviruses like DENV, JEV and CHIKV (X). To

further interrogate whether ZIKV induced autophagy, Hamel and collaborators used confocal microscopy to demonstrate coexpression of the viral envelope protein and the cytosolic microtubule-associated light chain 3 (LC3) -a mammalian homologue of yeast Apg8p-, which in it's lipidated state contributes to the closure of autophagosomes (X). Their results revealed that LC3 colocalized with ZIKV viral envelope protein; thus confirming that ZIKV is able to trigger its replication by induction of autophagy in cutaneous fibroblasts (X).

3.3.Melanocytes

The role of melanocytes has not been explored in ZIKV infection. However, it is widely known that these specialized cells residing in the epidermis display important immune and metabolic functions capable of influencing response to pathogens as well as contributing to the clinical manifestations of cutaneous infections (X). From an immunological standpoint, melanocytes are equipped to stand on the forefront of an initial viral insult, based on their capacity to attract and recruit immune cells such as neutrophils, macrophages and lymphocytes (X), as well as to their ability to act as phagocytic, antigen processing and antigen-presenting cells (X). In a similar fashion to keratinocytes and cutaneous fibroblasts, melanocytes also express PRRs, which after recognition of specific PAMPs stimulate the production of type 1 IFNs (X) thus exhibiting an important role in containment of viral infections.

On the other hand, melanocytes throughout the course of infection could also be responsible for the clinical manifestations of disease. Various viruses, including arboviruses such as the alphaviruses, are known to directly infect melanocytes disturbing their metabolic functions and thus originating the pigmentary changes seen usually in infants short after the vanishing of a maculopapular rash like in the case of CHIKV infection (X). One can speculate that the post-

inflammatory hypopigmentation frequently seen days after the acute ZIKV rash in some patients would share the same pathological basis in the melanocyte.

4. Clinical Features

As revealed by sero-epidemiological surveys ZIKV human infections are usually asymptomatic. The first descriptive case of the disease was reported in detail in 1956 after experimental inoculation in a healthy volunteer, who developed headaches 82 hours post-inoculation accompanied by fever that lasted 48 hours with no associated cutaneous signs or symptoms (X). Later in 1964, the disease was reported on another individual after occupational exposure and who did exhibit a characteristic maculopapular rash involving the face, neck, trunk, palms and soles, 24 hours after the onset of headaches and other non-specific symptoms such as malaise and back pain (X). However, it wasn't until the Yap State and French Polynesian outbreaks in 2007 that the classic combination of fever, rash, arthritis and/or arthralgia and/or myalgia, conjunctivitis, and fatigue, would come to define the most common clinical picture of the disease (X).

ZIKV infection usually recreates an influenza-like illness that is difficult to differentiate from other arboviral (Dengue, Chikungunya) or exanthematic (Measles, Rubella) viral diseases (X); and when clinically apparent, often exhibit mild forms of the disease (X). The incubation period usually ranges from 3 to 10 days with the duration of illness lasting about a week (X). In light of the most recent epidemic, the Pan American Health Organization (PAHO) issued interim case definitions based on data obtained from the current epidemic in the Region of the Americas (PAHO). Thus, a suspected case is a patient with a rash (usually pruritic and maculopapular) with two or more of the following signs or symptoms: an elevated body temperature (<38.5°C),

arthralgia or myalgia, nonpurulent conjunctivitis or conjunctival hyperemia, headache or malaise and peri-articular edema (PAHO). A confirmed case is a suspected case with a positive laboratory confirmation of ZIKV (PAHO).

The cardinal cutaneous manifestation of ZIKV infection is the maculopapular rash and prurtitis (X). However, in our experience there is a marked diversity in the characteristics of the rash as well as the severity of illness, ranging from a conspicuous, diffuse mildly pruritic maculopapular rash to cases with nearly universal erithrodermia. In the middle of the disease spectrum morbiliform-like rashes and exanthem-like eruptions with predominance of macules, plaques and patches (like those seen in CHIKV infection) are often seen. As opposed to CHIKV and DENV where the rash occurs generally after the fourth day of onset of symptoms, in ZIKV, cutaneous manifestations occur commonly in the first 24-to-48 hours after the onset of symptoms in over 90% of the cases (X).

Individual lesions are usually macules, papules, and plaques that can even appear as wheals. They are usually erythematous, round to oval, and arranged in combination patterns (maculo-papular most commonly) (X) or exhibiting a reticular (linear and net-shaped) appearance (X), and blanching on palpation (X). As for the distribution, lesions are usually generalized following a symmetrical pattern that commonly involves face, neck, trunk, palms and soles (X). In Venezuela however (data not published), a distinct pattern characterized by accentuation of the lesions in proximal areas of lower and upper limbs, neckline and abdomen has been observed in the majority of patients. Painful periarticular edema of the joints is also a distinctive sign (PAHO), occurring most commonly in small joints (X) of wrists and ankles, often in a symmetrical fashion.

Atypical cutaneous manifestations have also been described in ZIKV infection. Karimi et al. recently reported a case of ZIKV immune-mediated thrombocytopenia in a returning traveler from Surinam who developed generalized pruritus and a maculopapular rash 11 days after, subsequently developing swelling of the hand and wrists with subcutaneous haematomas on both arms and legs without preceding trauma (X). Similarly, Sharp et al. have reported the occurrence of thrombocytopenia in two patients exhibiting petechial and ulcerous lesions of the tongue and oral mucosa as well as ecchymotic lesions of the upper limb (X). Although uncommon, the occurrence of jaundice during ZIKV infection was also reported during the initial description of human cases in Nigeria in 1952 (X).

In a large study carried out on 72 ZIKV infected pregnant woman in Rio de Janeiro (Brazil), pruritus was present in 94% of the patients along with a maculopapular rash (X), highlighting the importance of cutaneous involvement in suggesting the possibility of ZIKV infection. Mucocutaneos and ophthalmologic involvement is not uncommon in ZIKV infected patients. Conjunctivitis is considered one of the most common signs (X), it is often non-purulent and frequently described as a conjunctival hyperemia (X). On the other hand, the occurrence of petechial lesions in the hard palate has been described (X) and also often seen by us in our ZIKV infected patients. Aphtous ulcers have also been reported to occur (X).

One interesting aspect that is worth commenting from our field experience in Venezuela is that most of the patients who usually exhibited severe, extensive rash unequivocally recalled having a previous episode of flavivirus infection (mostly Dengue), which is endemic in our country. It can be speculated that such phenomena could reflect the presence of enhancing antibodies causing an anamnestic response due to a previous flavivirus infection.

Also, the occurrence of psoriatic-like lesions in patients with no personal or family history of Psoriasis, weeks after acute ZIKV infection, is an interesting finding that prompts further and more elaborated studies. It is possible that genetic changes in ZIKV as noted previously for other arboviruses could be responsible for phenotypic changes influencing virulence and clinical outcome of some of these patients.

5. Differential Diagnosis

Considerations on the differential diagnostic approach, not only of ZIKV infection but other arbovirosis is challenging and must be based not only the type of cutaneous lesions but also on systemic signs and symptoms. An in depth understanding on the natural history of arboviral infections is pivotal since incubation period and onset of symptoms may differ widely or even overlap in some circumstances. For example, the incubation period for ZIKV, CHIKV and DENV may significantly superpose with a time range of 5-to10 days.

Knowledge on the endemic epidemiology is also an essential tool for diagnosis, because geographic restriction, seasonal behavior and distribution of certain viruses may hold the clue to narrow the list of suspects. It is also important to consider that the presence of vectors is highly influenced by climate and that vectorial transmission is crucial in the life cycle of these viruses.

A wide variety of infectious and non-infectious entities can course with fever and rash making diagnosis particularly challenging, with viral agents being the most common etiological source. Viral agents that should be considered in the list of differentials of ZIKV infection-like rash include: Arboviruses (WNV, CHIKV, DENV and MAYV), parvovirus, human herpesviruses, enteroviruses, rubella and measles, amongst others.

West Nile virus infection can exhibit a maculopapular rash, however lesions tend to be punctate, less confluent and more pronounced in the extremities (X). Neurological symptoms along with more severe systemic signs are important clues to its diagnosis. CHIKV on the other hand can reveal a myriad of cutaneous symptoms, being the morbiliform (maculopapular) rash it´s most common skin manifestation (X). The rash most commonly affects trunk and limbs and to a lesser extent face, palms and soles (X). Pruritus and desquamation may occur, and recrudescence of the rash days after the onset of initial symptoms has been described (X). In addition, CHIKV may also course with vesiculobullous, ecchymotic, and vasculitic-like purpuric lesions (X), as well as with transient nasal erythema, anogenital aphtous ulcers, generalized erythroderma and diffuse post-inflammatory hyperpigmentation (X). Tenderness and edema of hands and feet (X) is a shared feature with ZIKV. The occurrence of severe constitutional symptoms; especially arthralgia's usually suggests CHIKV over ZIKV infection.

DENV also exhibits a wide spectrum of symptoms that range from asymptomatic or mild undifferentiated febrile viral symptoms with or without morbiliform rash to sudden onset of fever, myalgias / arthralgias, retroorobital pain along with a diffuse maculopapular rash that may be pruritic and desquamate (X). However, in severe cases, skin hemorrhages and petechiae are usually observed (X).

Erythema infectiosum due to Parvovirus, also known as the fifth disease can present as a generalized confluent maculopapular eruption, however a key to its diagnosis is the intermittent nature of the rash which can last up to 3 weeks (X) and the accentuation of the eruption in cheeks (X). An important aspect to highlight is that in adults, Parvovirus B19 may cause arthralgias akin to those of caused by arthritogenic alphaviruses like CHIKV (X).

Human herpesviruses should also be considered in the list of differential diagnosis. In particular, human herpesvirus type 6 which causes a very similar maculopapular eruption to ZIKV, known as exanthema subitum or roseola infantum (X) lasting similarly 24-to-72 hours (X). Other members of the herpesviridae family like Cytomegalovirus (CMV) and human herpesvirus type 7 can also cause a nonspecific morbiliform or urticariform eruption that may pose a challenge at the time of diagnosis (X). Epstein-Barr virus (a *Gammaherpesvirinae*) is often associated with a maculopapular or urticarial rash; however it commonly is accompanied by classic symptomatology of infectious mononucleosis (tonsillitis, pharyngitis, lymph node enlargement and visceromegalys) often occurring after the administration of ampicillin (X). In addition petechial lesions, and occasionally jaundice may occur as well (X). Petechial lesions of the hard palate are indistinguishable from those seen in ZIKV.

In endemic areas ZIKV infection remains largely a childhood illness being often confused with other viral exanthems of childhood such as measles and rubella (X). Measles can be characteristically differentiated from a clinical perspective based on it´s well recognized prodromic phase (the triad of cough, coryza and conjunctivitis) and the appearance of erythematous facial macules and patches early in the course of disease that later follow a cephalocaudal confluent spread to trunk and extremeties (X).

Rubella (German measles) is of utmost importance being perhaps the most significant entity to consider in the differential when facing a pregnant patient proceeding from endo-epidemic areas of ZIKV. This is due to the significant overlap of clinical symptoms and their shared potential for vertical transmission and for causing congenital rubella and/or ZIKV syndrome (X).

Non-polio enteroviruses are also a cause of nonspecific exanthems, describing a variety of patterns such as scarlatiniform, urticarial, zosteiform and vesicular forms (X). Echoviruses, in particular Echovirus type 6 and 9 have been associated with variable rubelliform or morbilliform eruptions and low-grade fever that initially involve the face to later extend caudally to trunk and limbs (X). Echovirus 16 in particular causes a rubelliform-like eruption with discrete pink-red macules covering face and neck to the upper trunk and extremities, this characteristic roseola-like exanthem is classically known as the "Boston rash" (X).

Other less likely diagnoses that may resemble the ZIKV maculopapular rash include: adenoviral infection, unilateral laterothoracic exanthema, scarlet fever, rickettsial diseases (endemic typhus and Rocky Mountain spotted fever), Q fever, erlichiosis (X), Reovirus infection (X), Barmah forest virus (X), Ross river virus (X) and more rarely the new and old world hemorrhagic fevers (X).

The serologic approach to flavivirus diagnoses is often equivocal due to group-specific, complex-specific and subtype-specific cross-reactivities determined by the different domains of the envelope (E) protein.

6.1. Histopathology

Arboviral infections in general are frequently associated with a spectrum of cutaneous symptoms that can range from mild to severe clinical manifestations. However, from a histological standpoint changes in this group of infections have been poorly documented and are usually non-specific, frequently exhibiting a perivascular lymphocytic cell infiltrate (X). Nevertheless, in a recent experimental study performed to characterize the biology of ZIKV infection in human skin cells, Hamel et al. described a number of distinct histopathological features which include: Cytoplasmic keratinocyte vacuolation with presence of pyknotic nuclei, usually confined to the stratum granulosum, as well as the sporadic occurrence of edema which

is usually limited to the subcorneal layer (X). More recently, our group analyzed biopsies from ZIKV infected patients who volunteered for the study (data not published) confirming Hamel's group findings, while providing further insights into pathological findings.

The histological features vary according to the nature of the cutaneous lesion. Biopsies obtained from a classic erythematous maculo-papular rash usually reveal a non-specific lymphocytic dermal infiltrate, often perivascular and superficial. Biopsies from macular and patch-like lesions usually show slight acanthosis, focal spongiosis and in three cases we observed erythrocyte extravasation and slight papillary dermal edema. Variable degree of spongiosis, focal exocytosis of lymphocytes into the epidermis and focal dyskeratosis were observed in confluent macular lesions (mimicking those observed in CHIV).

Conclusions:

Lessons learned from what has been observed in the recent outbreak in the Americas have been useful in guiding efforts to help recognize from a clinical standpoint ZIKV disease and its potential complications. Despite a significant clinical overlap with other viral exanthems, the skin still holds pathognomonic clues in recognizing ZIKV cutaneous disease.

LIST OF REFERENCES

Alizon, S. and van Baalen, M. 2005. Emergence of a convex trade-off between transmission and virulence. American Naturalist, 165: E155--E167.

Balm MN, Lee CK, Lee HK et al. A diagnostic polymerase chain reaction assay for Zika virus. J Med Virol 2012; 84:1501–5.

Bangham, J., Kim, K.W., Webster, C.L. and Jiggins, F.M. 2008. Genetic variation affecting host-parasite interactions: Different genes affect different aspects of sigma virus replication and transmission in *Drosophila melanogaster*. Genetics, 178: 2191-2199.

Bangham, J., Obbard, D.J., Kim, K.W., Haddrill, P.R. and Jiggins, F.M. 2007. The age and evolution of an antiviral resistance mutation in *Drosophila melanogaster*. Proceedings of the Royal Society Biological Sciences, 274: 2027-2034.

Bjornstad, O.N., Finkenstadt, B.F. and Grenfell, B.T. 2002. Dynamics of measles epidemics: Estimating scaling of transmission rates using a Time series SIR model. Ecological Monographs, 72: 169-184.

Borer, E.T, E.W. Seabloom, C.E. Mitchell, A.G. Power. 2010. Local context drives infection of grasses by vector-borne generalist viruses. Ecology Letters 13(7): 810-818.

Brun, G. and Plus, G. 1980. The Viruses of Drosophila (trans.) A. Ashburner and T.R.F. Wright. In The Genetics and Biology of Drosophila (A. Ashburner and T.R.F. Wright, eds), The Genetics and Biology of Drosophila, pp. 625-702. London: Academic Press.

Buckner, E.A., B.W. Alto, L.P. Lounibos. 2013. Vertical Transmission of Key West Dengue-1 Virus by Aedes aegypti and Aedes albopictus (Diptera: Culicidae) Mosquitoes from Florida. Journal of Medical Entomology. 50(6): 1291–1297.

Carpenter, J., Hutter, S., Baines, J.F., Roller, J., Saminadin-Peter, S.S., Parsch, J. and Jiggins, F.M. 2009. The transcriptional response of *Drosophila melanogaster* to infection with the sigma virus (rhabdoviridae). Plos One, 4. Sedlacek, W. E. (1999). Black students on White campuses: 20 years of research. *Journal of College Student Development, 40*(5), 538-549.

Carpenter, J.A., Obbard, D.J., Maside, X. and Jiggins, F.M. 2007. The recent spread of a vertically transmitted virus through populations of *Drosophila melanogaster*. Mol. Ecol., 16: 3947-3954.

Combes, C. 2001. Parasitism: The Ecology and Evolution of Intimate Interactions. Chicago: University of Chicago Press.

Crowder, DW, EA Dykstra, JM Brauner et al. (2013) West Nile Virus Prevalence across Landscapes Is Mediated by Local Effects of Agriculture on Vector and Host Communities. PLoS One. http://dx.doi.org/10.1371/journal.pone.0055006

Dahari H., R.M. Ribeiro, C.M. Rice, A.S. Perelson. 2007. Mathematical Modeling of Subgenomic Hepatitis C Virus Replication in Huh-7 Cells Journal of Virology 81(2): 750–760.

Dejnirattisai, W, P. Supasa, W. Wongwiwat, A. Rouvinski et al. (2016) Dengue virus sero-cross-reactivity drives antibody-dependent enhancement of infection with zika virus. Nature Immunology 17, 1102–1108

Ebert, D. 1999. The evolution and expression of parasite virulence. In Evolution in Health & Disease (S.C. Stearns, ed), pp. 161-172. New York: Oxford University Press.
Ebert, D. and Bull, J.J. 2003. Challenging the trade-off model for the evolution of virulence: is virulence management feasible? Trends in Microbiology, 11: 15-20.

Félix, R., Guzmán, J. and de Garay Arellano, A. 1971a. Distribution of CO2 sensitivity (sigma virus) in an urban population of D. melanogaster from Mexico City. II. Low dispersal, a factor which explains differences among locations. Drosophila Information Service, 47: 105-109.

Félix, R., Gúzman, J. and de Garay Acellano, A. 1971b. Carbon dioxide sensitivity of Drosophilid flies from a location in the outskirts of Mexico City. Drosophila Information Service, 47: 110-112.

Ferguson, J.M. and J.M. Ponciano. 2014. Predicting the process of extinction in experimental microcosms and accounting for interspecific interactions in single-species time series. Ecology Letters 17: 251-259.

Ferguson, J., Carvalho, F., Murillo, O. and J.M. Ponciano. 2015a. Population growth, density dependence and evironmental autocorrelation in animal populations. Theoretical Ecology, 8(2):doi 10.1007/s12080-015-0276-6

Ferguson, J.M. and J.M. Ponciano. 2015b. Evidence and implications of higher order scaling in the environmental variation of animal population growth. Proceedings of the National Academy of Sciences. 112(9): doi: 10.1073/pnas.1416538112.

Fine, P.E.M. 1975. Vectors and vertical transmission: an epidemiological perspective. Annals of the New York Academy of Sciences, 266: 173-194.

Fleuriet, A. 1976. Presence of the hereditary rhabdovirus sigma and polymorphism for a gene for resistance to this virus in natural populations of *Drosophila melanogaster*. Evolution, 30: 735-739.

Fleuriet, A. 1980. Polymorphism of the hereditary sigma virus in natural populations of *Drosophila melanogaster*. Genetics, 95: 459-465.

Fleuriet, A. 1981. Comparison of various physiological traits in flies (*Drosophila melanogaster*) of wild origin, infected or uninfected by the hereditary Rhabdovirus sigma. Arch. Virol., 69: 261-272.

Fleuriet, A. 1996. Polymorphism of the *Drosophila melanogaster* - Sigma virus system. Journal of Evolutionary Biology 9: 471-484.

Gay, P. 1978. Les genes de la drosophile qui interviennent dans la multiplication du virus sigma. Mol. Gen. Genet., 159: 269-283.

Goddard, L.B., Roth, A.E., Reisen, W.K. and Scott, T.W. 2003. Vertical transmission of West Nile virus by three California Culex (Diptera : Culicidae) species. Journal Of Medical Entomology, 40: 743-746.

Goldstein, L. 1949. A mutant genoid in Drosophila that is sensitive to Carbon Dioxide. Nature, 164: 369- 369.

Hotez P.J., M.G. Basáñez, A. Acosta-Serrano, M.E. Grillet. 2017. Venezuela and its rising vector-borne neglected diseases. PLoS Negl Trop Dis 11(6): e0005423. https://doi.org/10.1371/journal.pntd.0005423

Inouye, B.D. 2005. The importance of the variance around the mean effect size of ecological processes: Comment. Ecology, 86: 262-265.

Jones, K.E., N.G. Patel, M.A. Levy, A. Storeygard, D. Balk, J.L. Gittleman, P. Daszak. 2008. Global trends in emerging infectious diseases. Nature 451 (7181): 990-993

Lafferty, K. D., A.M. Kuris 2009. Parasitic castration: The evolution and ecology of body snatchers. Trends in Parasitology, 25, 564–572

Lee, KP, SJ Simpson, K Wilson. Dietary protein-quality influences melanization and immune function in an insect. Functional Ecology 2008, 22, 1052– 1061

Lloyd-Smith, J.O., George, D., Pepin, K.M., Pitzer, V.E., Pulliam, J.R.C., Dobson, A.P., Hudson, P.J., Grenfell, B.T. 2009. Epidemic dynamics at the human-animal interface. Science 326(5958): 1362-1367.

L'Héritier, P. 1958. The hereditary virus of Drosophila. Advances in Virus Research, 5: 195-245.

L'Héritier, P. 1970. Drosophila viruses and their role as evolutionary factors. Evol. Biol., 4: 185-209.

L'Héritier, P. and Teissier, G. 1945. Transmission héréditaire de la sensibilité au gaz carbonique chez la Drosophile. Publ. lab. ENS Biologie, 1: 35-76.

Longdon, B., Obbard, D.J. and Jiggins, F.M. 2010. Sigma viruses from three species of Drosophila form a major new clade in the rhabdovirus phylogeny. Proceedings of the Royal Society Biological Sciences, 277: 35-44.

Lord, C. C., B.W. Alto, S.L Anderson, C.R. Connelly, J.F. Day, S.L Richards, C.T Smartt, W.J. Tabachnik. 2014. Can Horton Hear the Whos? The Importance of Scale in Mosquito-Borne Disease. Journal of Medical Entomology, 51(2): 297-313.

Mangin, K.L., Lipsitch, M. and Ebert, D. 1995. Virulence And transmission modes of 2 microsporidia in Daphnia-Magna. Parasitology, 111: 133-142.

Mayer, S.V, R.B. Tesh, N. Vasilakis. 2017. The emergence of arthropod-borne viral diseases: A global prospective on dengue, chikungunya and zika fevers. Acta Tropica 166: 155-163

Mishra, A.C. and Mourya, D.T. 2001. Transovarial transmission of West Nile virus in Culex vishnui mosquito. Indian Journal of Medical Research, 114: 212-214.

Morris, W.F. 1997. Disentangling effects of induced plant defenses and food quantity on herbivores by fitting nonlinear models. American Naturalist, 150: 299-327.

Murray, K.O., Mertens, E. and Despres, P. 2010. West Nile virus and its emergence in the United States of America. Veterinary Research, 41.

Padmanabhan P, NM Dixit. 2011. Mathematical Model of Viral Kinetics In Vitro Estimates the Number of E2-CD81 Complexes Necessary for Hepatitis C Virus Entry. PLoS Computational Biology 7(12): e1002307. https://doi.org/10.1371/journal.pcbi.1002307

Patterson, J., M. Sammon, M. Garg 2016. Dengue, Zika and Chikungunya: Emerging Arboviruses in the New World. West J Emerg Med. 17(6): 671–679.

Peck, GW and WE Walton (2005) Effect of Different Assemblages of Larval Foods on Culex quinquefasciatus and Culex tarsalis (Diptera: Culicidae) Growth and Whole Body Stoichiometry. Environmental Entomology 34(4):767-774. 2005

Perera, R, M Khaliq, RJ Kuhn. (2008) Closing the door on flaviviruses: Entry as a target for antiviral drug design. Antiviral Research 80:11-22

Read A. F. (1994). The evolution of virulence. Trends in Microbiology 2:73–76

Reisen, WK. (2013) Ecology of West Nile Virus in North America. Viruses, 5, 2079-210

Romero-Brey, I. and R. Bartenschlager 2016. Endoplasmic Reticulum: The Favorite Intracellular Niche for Viral Replication and Assembly. Viruses 8(6): 160.

Root, J.J. 2013. West Nile Virus associations in wild mammals: a synthesis. Archives of Virology 158:735–752

Sall, A.A., Faye, O., Diallo, M., Firth, C., Kitchen, A. and Holmes, E.C. 2010. Yellow fever Virus exhibits slower evolutionary dynamics than dengue virus. Journal of Virology, 84: 765-772.

Sterner, R. W., & Elser, J. J. (2002). Ecological stoichiometry: The biology of elements from Molecules to the biosphere. Princeton: Princeton University Press.

Turell MJ, Dohm DJ, Sardelis MR, Oguinn ML, Andreadis TG, Blow JA. An update on the potential of north American mosquitoes (Diptera: Culicidae) to transmit West Nile Virus. J Med Entomol. 2005;42(1):57-62.

Vieira de Morais Bronzoni, R, FG Baleotti, RM Ribeiro Nogueira, M Nunes, L Tadeu Moraes Figueiredo (2005) Duplex Reverse Transcription-PCR Followed by Nested PCR Assays for Detection and Identification of Brazilian Alphaviruses and Flaviviruses. Journal of Clinical Microbiology: 43(2); 696–702

WHO. Zika virus, Microcephaly, and Guillain Barré Syndrome Situation Report. 25 August 2016.WebLink

Wayne, M.L., Contamine, D. and Kreitman, M. 1996. Molecular population genetics of ref(2)P, a locus which confers viral resistance in Drosophila. Mol. Biol. Evol., 13: 191-199.

Wayne, M.L., Telonis-Scott, M., Bono, L.M., Harshman, L., Kopp, A., Nuzhdin, S.V. and McIntyre, L.M. 2007. Simpler mode of inheritance of transcriptional variation in male *Drosophila melanogaster*. Proceedings of the National Academy of Sciences of the United States of America, 104: 18577-18582.

Weaver, S.C., W.K. Reisen 2010 Present and Future Arboviral Threats. Antiviral Research 85(2): 328.

Wilfert, L. and Jiggins, F.M. 2010a. Disease association mapping in Drosophila can be replicated in the wild. Biology Letters, 6: 666-668.

Wilfert, L. and Jiggins, F.M. 2010b. Host-parasite coevolution: genetic variation in a virus population and the interaction with a host gene. Journal of Evolutionary Biology, 23: 1447-1455.

Williamson, D.L. 1961. Carbon dioxide sensitivity in Drosophila affinis and D. athabasca. Genetics, 46:1053-1060.

Yampolsky, L.Y., Webb, C.T., Shabalina, S.A. and Kondrashov, A.S. 1999. Rapid accumulation of a vertically transmitted parasite triggered by relaxation of natural selection among hosts. Evolutionary Ecology Research, 1: 581-589

Zambrano Y, A Chiarello, A Soca, I Villalobos, M Marrero, M Soler, J Laferte, M Alvarez. Use Of polymerase chain reaction for the diagnosis of central nervous system infections. Invest Clin 2006; 47(4):337-47

Zlotnick, A, S. Mukhopadhyay 2011. Virus assembly, allostery, and antivirals. Trends in Microbiology. 19(1): 14–23.

BIOGRAPHICAL SKETCH

Gabriela Blohm earned her BSc in wildlife ecology, and MSc in zoology at the University of Florida. She has studied a broad range of ecological systems and will be directing her research efforts towards the control of vector-borne diseases in her home country. She hopes to continue her career as a research biologist with a focus on public health and wildlife disease surveillance in Venezuela. Her long-term goal is to work with biologists, epidemiologists and health care practitioners to develop strategies for improving public health in Venezuela, with a focus on reducing the spread of mosquito-borne viruses in areas where water quality control measures are not in place and where fertilizer use is unregulated.

She also plans to continue working with her family on the management of a cattle ranch and research station in central Venezuela. Researchers and staff at Masaguaral, the ranch, have continued a 42 year-long research program that has resulted in more than 500 peer-reviewed scientific publications and 30 years of hands-on education for students in veterinary medicine and crocodilian conservation.